J Membrane Biol (2010) 235:191–210
DOI 10.1007/s00232-010-9266-1

Differential Regulation of Calcium-Activated Potassium Channels by Dynamic Intracellular Calcium Signals

Joanne E. Millership · Caroline Heard · Ian M. Fearon · Jason I. E. Bruce

Received: 10 October 2009 / Accepted: 14 May 2010 / Published online: 11 June 2010

Abstract Calcium (Ca^{2+})-activated K^+ (K_{Ca}) channels regulate membrane excitability and are activated by an increase in cytosolic Ca^{2+} concentration ($[Ca^{2+}]_i$), leading to membrane hyperpolarization. Most patch clamp experiments that measure K_{Ca} currents use steady-state $[Ca^{2+}]$ buffered within the patch pipette. However, when cells are stimulated physiologically, $[Ca^{2+}]_i$ changes dynamically, for example during $[Ca^{2+}]_i$ oscillations. Therefore, the aim of the present study was to examine the effect of dynamic changes in $[Ca^{2+}]_i$ on small (SK3), intermediate (hIK1), and large conductance (BK) channels. HEK293 cells stably expressing each K_{Ca} subtype in isolation were used to simultaneously measure agonist-evoked $[Ca^{2+}]_i$ signals, using indo-1 fluorescence, and current/voltage, using perforated patch clamp. Agonist-evoked $[Ca^{2+}]_i$ oscillations induced a corresponding K_{Ca} current that faithfully followed the $[Ca^{2+}]_i$ in 13–50% of cells, suggesting a good synchronization. However, $[Ca^{2+}]_i$ and K_{Ca} current was much less synchronized in 50–76% of cells that exhibited Ca^{2+}-independent current events (55% of SK3-, 50% of hIK1-, and 53% of BK-expressing cells) and current-independent $[Ca^{2+}]_i$ events (18% SK3- and 33% of BK-expressing cells). Moreover, in BK-expressing cells, where $[Ca^{2+}]_i$ and K_{Ca} current was least synchronized, 36% of total $[Ca^{2+}]_i$ spikes occurred without activating a corresponding K_{Ca} current spike, suggesting that BK_{Ca} channels were either inhibited or had become desensitized. This desynchronization between dynamic $[Ca^{2+}]_i$ and K_{Ca} current suggests that this relationship is more complex than could be predicted from steady-state $[Ca^{2+}]_i$ and K_{Ca} current. These phenomena may be important for encoding stimulus–response coupling in various cell types.

Keywords Calcium activated potassium channels · Calcium oscillations · Dynamic calcium signaling · Ion channels · Electrophysiology

J. E. Millership · C. Heard · I. M. Fearon · J. I. E. Bruce (✉)
Faculty of Life Sciences, University of Manchester,
2nd Floor Core Technology Facility, 46 Grafton Street,
Manchester M13 9NT, UK
e-mail: jason.bruce@manchester.ac.uk

Calcium-activated potassium (K_{Ca}) channels are activated by an increase in intracellular calcium ($[Ca^{2+}]_i$), allowing potassium (K^+) efflux and cell hyperpolarization. K_{Ca} channels are found in many excitable and nonexcitable cell types and have a functional role in regulation of neuronal action potential firing (Faber and Sah 2003), cell proliferation (Wiecha et al. 1998), epithelial fluid secretion (Melvin et al. 2005), and regulation of vascular tone and thus blood pressure (Ledoux et al. 2006). There are three major subtypes of K_{Ca} channels that can be categorized by their respective conductances. These are termed large (BK), intermediate (IK), and small (SK) conductance channels. All three major subtypes are encoded by two families of genes termed *KCNN* and *KCNMA* families. SK1, SK2, and SK3 are encoded by *KCNN1, KCNN2,* and *KCNN3* genes, respectively, whereas IK (sometimes referred to as SK4 or IK1) is encoded by the *KCNN4* gene. Finally, BK is encoded by the *KCNMA1* gene (sometimes called *Slo*) (Gutman et al. 2003; Stocker 2004). Each subtype exhibits differing biophysical and pharmacological properties, tissue distributions, and functions. BK can be regulated by both voltage and Ca^{2+}, whereas SK and IK are regarded as essentially voltage independent (Gribkoff et al. 2001; Stocker 2004). Their activation by Ca^{2+} is also mechanistically differently; Ca^{2+} activation of SK and IK occurs via indirect binding of Ca^{2+} to calmodulin, whereas

Ca^{2+} activation of BK is via direct binding of Ca^{2+} to Ca^{2+} binding motifs. Moreover, BK channels are voltage dependent and can be regulated by the coexpression of the β subunit, both of which can affect the Ca^{2+} sensitivity (Cox and Aldrich 2000; Latorre and Brauchi 2006; Perez et al. 1993; Petrik and Brenner 2007; Wallner et al. 1995). Furthermore, single-channel studies have shown that BK channels from rat hippocampal neurons undergoe Ca^{2+}-dependent inactivation at concentrations as low as 1 μM (Hicks and Marrion 1998). The coexpression of specific β subunits (e.g., β2 and β3) with BK also results in a similar fast inactivation (Brenner et al. 2000a; Lippiat et al. 2003; Wallner et al. 1999). This is likely to be responsible for the Ca^{2+}-dependent inactivation of BK reported in hippocampal neurons (Hicks and Marrion 1998), suggesting a complex regulation of BK by Ca^{2+} and different β subunits. Each BK gene can also undergo splicing and results in multiple splice variants that exhibit differential tissue distribution, Ca^{2+} sensitivity, and regulation by downstream signaling pathways. The two most commonly studied splice variants of BK are ZERO, which contains no insert, and STREX (stress-regulated exon), which contains a 51-amino acid cysteine-rich insert that renders BK more sensitive to Ca^{2+} (Chen et al. 2005; Erxleben et al. 2002; Saito et al. 1997).

Intracellular Ca^{2+} ($[Ca^{2+}]_i$) signals are able to control many different cellular processes because cells are able to generate $[Ca^{2+}]_i$ oscillations with varying amplitudes, frequency, and spatial properties, which help to encode stimulus–response coupling (Berridge et al. 2003). This diversity of $[Ca^{2+}]_i$ signaling enables specific effectors to be activated differentially by specific patterns of spatiotemporal $[Ca^{2+}]_i$ signals in response to different stimuli and sometimes within the same cell. For example, in T lymphocytes, the frequency of $[Ca^{2+}]_i$ oscillations has been shown to differentially regulate Ca^{2+}-dependent transcription factors, NFAT (nuclear factor of activated T cells), Oct/OAP (octamer-binding factor/octamer-associated protein), and NF-κB (nuclear factor κB), important during the immune response (Dolmetsch et al. 1998). Similar $[Ca^{2+}]_i$ oscillation-dependent mechanisms may exist in endothelial cells (ECs), whereby different agonists that couple to $[Ca^{2+}]_i$ signaling can produce varying magnitude hyperpolarization and thus arteriolar vasodilation (Brahler et al. 2009; Crane et al. 2003; Frieden et al. 2002; Marchenko 2002; Sankaranarayanan et al. 2009). This could be due to differential regulation of K_{Ca} channels by different spatiotemporal patterns of $[Ca^{2+}]_i$ signaling, although further studies are needed to confirm this.

Most studies examining the Ca^{2+} sensitivity of K_{Ca} channels have used steady-state concentration of Ca^{2+}, for example by buffering the patch pipette solution to set concentrations to determine the Ca^{2+} dependency of both whole-cell and single-channel K_{Ca} currents (Ahring et al. 1997; Barfod et al. 2001; Cox and Aldrich 2000; Erxleben et al. 2002; Hirschberg et al. 1998; Ishii et al. 1997; Joiner et al. 1997; Kohler et al. 1996; Logsdon et al. 1997; Xia et al. 1998). By means of these techniques, IK has been reported to be the most Ca^{2+} sensitive with an EC_{50} of ~100–300 nM (Ishii et al. 1997; Joiner et al. 1997; Logsdon et al. 1997), SK with an EC_{50} of ~600–700 nM (Barfod et al. 2001; Hirschberg et al. 1998; Kohler et al. 1996; Xia et al. 1998), BK is the least Ca^{2+} sensitive with an EC_{50} of > 1 μM (Ahring et al. 1997; Erxleben et al. 2002; Petrik and Brenner 2007), although this depends on the voltage, the BK splice variant, and the presence of the β subunits (Cox and Aldrich 2000; Faber and Sah 2003; Latorre and Brauchi 2006; Petrik and Brenner 2007). However, when cells are stimulated physiologically, $[Ca^{2+}]_i$ very rarely reaches a steady state, but instead changes dynamically, for example during $[Ca^{2+}]_i$ oscillations. Although the biophysical and Ca^{2+} dependency of K_{Ca} channels have been widely studied, it remains largely unknown how dynamic changes in $[Ca^{2+}]_i$ regulate these channels.

The aim of the present study was to test the hypothesis that different temporal patterns of $[Ca^{2+}]_i$ signals differentially regulate K_{Ca} channel activity, and as a result of their differing Ca^{2+} sensitivities and mechanisms of Ca^{2+} activation, different K_{Ca} channel subtypes respond differently to temporally distinct patterns of dynamic $[Ca^{2+}]_i$ signals. Such differential regulation of K_{Ca} channels would allow cells to encode for electrical activity by subtle differences in the pattern of agonist or stimulus-evoked $[Ca^{2+}]_i$ signaling.

Materials and Methods

Cell Culture and Stable Transfections

Untransfected HEK293 cells were provided by Frank Graham, McMaster University, and HEK293 M3 cells were from Gary Willars, University of Leicester. BK_{STREX} DNA (stress-regulated exon BK splice variant) was a gift from Mike Shipston, University of Edinburgh. HEK293 hIK1 cells were a gift from Dan Devor, University of Pittsburgh, and HEK293 SK3 cells were a gift from Steve Lidofsky, University of Vermont.

HEK293 cells were cultured in minimum essential medium containing Earle salts and L-glutamine, supplemented with 10% fetal bovine serum, 1% nonessential amino acids, and 1% antibiotic/antimycotic (all purchased from Gibco, Invitrogen Ltd, Paisley, UK). Selection for HEK293 BK and HEK293 hIK1 was maintained with 600 μg/ml G418 disulfate (Sigma-Aldrich, Gillingham, Dorset, UK) and selection for HEK293 SK3 was

maintained with 200 μg/ml hygromycin B (Sigma-Aldrich, Gillingham, Dorset, UK). Cells were passaged every 3 to 4 days once they had reached approximately 70% confluency and were incubated at 37°C in a 5% CO_2 humidified atmosphere. HEK293 cells were transfected with ExGen 500 (Fermentas, York, UK) in vitro transfection reagent according to the manufacturer's instructions. The rat liver SK3 was subcloned from pPCR-Script into the mammalian expression vector, pTracer-CMV2 (Invitrogen Ltd, Paisley, UK), via *Eco*RI and *Not*I restriction sites (Barfod et al. 2001). The IK1 channel was subcloned from pBF plasmid into pcDNA3.1(+) by using *Eco*RI and *Xho*I restriction sites (Jones et al. 2005). Finally, BK_{STREX} was subcloned into pcDNA3.1 + zeo for expression into HEK293 (Erxleben et al. 2002; Shipston et al. 1999). One day after transfection, 0.6 mg/ml of the G418 disulfate (or 0.2 mg/ml zeocin for BK_{STREX}) selection antibiotic was added to each stable cell line. Transfected cells were kept under selection for 2 to 3 weeks and the media changed every 3 to 4 days before picking of individual round colonies that were transferred to new dishes. Each colony was further trypsinized and cultured to 70% confluence and split further for functional screening by measuring the whole-cell currents. After a second round of screening, one colony was selected for passaging and used in further experiments.

Cells were seeded on 25-mm glass coverslips for $[Ca^{2+}]_i$ imaging experiments, or in 35-mm dishes for electrophysiology experiments. HEK293 M3 cells were transfected with DNA encoding a green fluorescent protein-tagged BK channel.

Measurement of $[Ca^{2+}]_i$ Using Fura-2 and Indo-1 Fluorescence

Initial experiments characterizing agonist-evoked $[Ca^{2+}]_i$ responses in untransfected HEK293 cells utilized fura-2 imaging. However, when $[Ca^{2+}]_i$ and membrane potential/current were measured simultaneously, changes in $[Ca^{2+}]_i$ were monitored using indo-1 and a photomultiplier-based detection system. HEK293 cells were seeded on 25-mm glass coverslips overnight before loading with 3 μM fura-2 AM or 2.5 μM indo-1 AM in HEPES-PSS for 30 min at room temperature. Cells were then washed and incubated for 30 min in dye-free HEPES-PSS at 37°C and 5% CO_2 to allow de-esterification of the dye. The coverslips formed the base of a gravity-fed perfusion chamber whereby solutions were rapidly changed using automatic valves (Harvard Apparatus, Kent, UK).

Measurement of Fura-2 Fluorescence

Cells were observed on an inverted microscope (Nikon Eclipse TE2000-S), using a Nikon 40X oil immersion objective. Fura-2-loaded cells were excited using a xenon arc lamp (Cairn Research, Kent, UK) at 340 and 380 nm (± 10 nm bandwidth for each wavelength) and alternately via a monochromator (Cairn Research, Kent, UK). The emitted fluorescence (at 510 nm) was separated from excitation light using a 400-nm dichroic mirror (DM400, Chroma, Bellows Falls, VA, USA) and a 510-nm broadband emission filter. Background-subtracted 340- and 380-nm fluorescence images were acquired every second by a CoolSNAP HQ CCD camera (Photometrics, Tucson, AZ, USA) controlled and processed by Metafluor image acquisition and analysis software (Molecular Devices, CA, USA). All hardware described above was purchased from Cairn Research, Kent, UK. F340/F380 ratiometric images were processed off-line. All experiments were performed at room temperature.

Measurement of Indo-1 Fluorescence

Cells were seeded on 25-mm glass coverslips that were mounted within a perfusion chamber on the stage of an inverted microscope (Olympus IX71) and observed using a Nikon 40X oil immersion objective. Individual cells were selected using a manual diaphragm (Cairn Research, Kent, UK) and were excited with a mercury lamp (Burleigh Exfo, ON, Canada) at 360 nm for 100 ms every second using a shutter to avoid bleaching. The emitted fluorescence at 405 nm and 485 nm was passed through a dichroic filter and captured with a photomultiplier tube (Cairn Research, Kent, UK). Amplified signals were digitized using a Digidata 1322A interface, recorded using pCLAMP 9.2 software (Axon Instruments-Molecular Devices, Tucson, AZ, USA), and the F_{405}/F_{485} ratio was determined. All the above hardware were purchased from Scientifica UK, East Sussex, UK. As a result of technical difficulties, not every cell in which both $[Ca^{2+}]_i$ and K_{Ca} current (or membrane potential) was simultaneously measured could be calibrated to give "true" $[Ca^{2+}]_i$. Therefore, all traces depict the uncalibrated F_{405}/F_{485} ratio as a measure of $[Ca^{2+}]_i$. However, average values were obtained from periodic in situ calibration experiments throughout the study to provide "estimated" $[Ca^{2+}]_i$ and are indicated within the figures and throughout the text. Indo-1 fluorescence was calibrated into estimated $[Ca^{2+}]_i$ by the following equation: $[Ca^{2+}]_i = K_d(R - R_{min})/(R_{max} - R)(S_{F485}/S_{B485})$ (Grynkiewicz et al. 1985), where K_d is the indo-1 dissociation constant (250 nM) (Grynkiewicz et al. 1985), R is any given 405/485 ratio value, S_{F485}/S_{B485} is the ratio of fluorescence measured at 485 nm for Ca^{2+}-free and Ca^{2+}-bound indo-1, and R_{min} and R_{max} are the minimum and maximum ratio values after in situ calibration experiments. This involved treating cells with 10 μM ionomycin, 0.5 μM carbonyl cyanide *m*-chlorophenylhydrazone (to prevent mitochondrial Ca^{2+} uptake), and 30 μM cyclopiazonic acid

(CPA; to prevent Ca^{2+} uptake into the endoplasmic reticulum [ER]) in Ca^{2+}-free HEPES-PSS (with 1 mM EGTA) to obtain R_{min} values and Ca^{2+}-saturated media (2 mM Ca^{2+}) to obtain R_{max} values. All experiments were carried out at room temperature (20–22°C).

Electrophysiology

The electrophysiological and pharmacological properties of untransfected HEK293, HEK293 SK3, HEK293 hIK1, and HEK293 BK cells were characterized using the whole-cell patch clamp technique. Cells were continuously perfused with an extracellular salt solution containing (mM): 140 NaCl, 4 KCl, 1 $CaCl_2$, 2 $MgCl_2$, 1 KH_2PO_4, 10 HEPES, 10 glucose, pH 7.4 with NaOH. Pipettes were filled with an intracellular solution containing (mM): 135 KCl, 5.53 $MgCl_2$, 0.207 $CaCl_2$, 10 HEPES and either 5 or 15.6 HEDTA (hydroxyethyl ethylenediamine triacetic acid), pH 7.2 with KOH. The different concentrations of HEDTA gave either 3 μM or 100 nM free Ca^{2+}, respectively (calculated using Webmaxc standard; http://maxchelator.stanford.edu/).

Cells were voltage clamped at −60 mV, and whole-cell currents were activated by a voltage ramp protocol (−110 mV to 110 mV, 200-ms duration). Current–voltage relationships were determined by a voltage step protocol (−100 mV to 110 mV in 10-mV increments, 100 ms per step). The effect of known pharmacological blockers (apamin, TRAM-34, iberiotoxin) and openers (riluzole, EBIO, NS1619) on whole-cell currents were assessed by addition of the agent to the extracellular solution. Membrane potential recordings were performed using a current clamp protocol (I = 0). The membrane potential of HEK293 SK3 cells was measured before, during, and after application of 300 μM riluzole. The pipette solution contained either 100 nM or 3 μM free Ca^{2+} to mimic channel activity at rest and during maximum stimulation, respectively.

Simultaneous Measurement of $[Ca^{2+}]_i$ and K_{Ca} Channel Activity

The perforated patch clamp technique was used to simultaneously measure membrane potential or membrane current and $[Ca^{2+}]_i$ during dynamic changes in $[Ca^{2+}]_i$ evoked by Ca^{2+}-mobilizing agonists. This technique allowed the intracellular environment of the cell to remain intact and allows intracellular signaling to be studied while still offering good electrical access to the cell (Horn and Marty 1988). Indo-1-loaded cells grown on coverslips that formed the base of a perfusion chamber were mounted onto the stage of the Olympus IX71 inverted microscope. Pipettes were filled with intracellular solution containing (mM) 5 NaCl, 135 KCl, 10 HEPES, pH 7.2 with KOH and contained 250–500 μg/ml nystatin (Sigma) to perforate the cell membrane. Membrane current or potential recordings were made once a seal had formed and the access resistance had reached <50 MΩ, which took 10–30 min.

Membrane currents were recorded at a holding potential of −60 mV using a voltage clamp protocol, while membrane potential recordings were made using a current clamp protocol (I = 0). After establishment of a stable baseline recording, either 30 μM carbachol or in some cells (HEK293 hIK1 cells) 10 μM histamine was applied to the cells to evoke dynamic changes in $[Ca^{2+}]_i$. Membrane currents and membrane potentials were recorded using a Multiclamp 700B amplifier, with a Digidata 1322A interface and pCLAMP 9.2 software (Axon Instruments-Molecular Devices, Tucson, AZ, USA). Data were analyzed off-line by Clampfit 9.2 (Axon Instruments-Molecular Devices, Tucson, AZ, USA) and represented graphically by Origin 6.1 (OriginLab). All the above hardware was purchased from Scientifica UK, East Sussex, UK.

Reagents

ATP, carbachol, histamine, bradykinin, TRAM-34, riluzole, and NS1619 were purchased from Sigma. EBIO and iberiotoxin were purchased from Tocris.

Statistical Analysis

Where statistics were used to compare two groups, an unpaired *t*-test was performed on data that were normally distributed (data that passed the Kolmogorov–Smirnov test), whereas a Mann–Whitney rank sum test was performed on data that were not normally distributed. When comparing the number of observations that fell within a given category, the χ^2 test was used. P values of < 0.05 were considered significant.

Results

Establishing a Model Cell System

Many cells that endogenously express K_{Ca} channels express a wide variety of other ion channels and often differentially express multiple types of K_{Ca} channels, thereby making analysis and interpretation of results complicated. In order to study each K_{Ca} channel subtype in isolation, it was therefore necessary to overexpress each recombinant K_{Ca} channel subtype in HEK293 cells that represent a null background for K_{Ca} expression. In order to study the effect of dynamic $[Ca^{2+}]_i$ signaling on K_{Ca}-expressing HEK293 cells, $[Ca^{2+}]_i$ signals in response to several endogenous receptor agonists (ATP, carbachol, bradykinin, and histamine) were characterized in untransfected HEK293 cells.

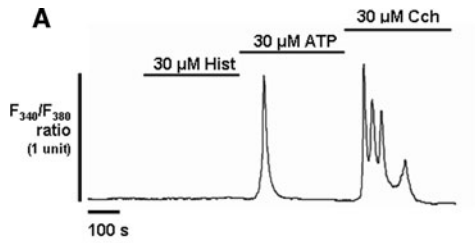

B

Agonist (30 μM)	Number of cells showing response	% of cells responding
ATP	59/87	68
Carbachol	75/84	89
Histamine	1/80	1
Bradykinin	2/36	6

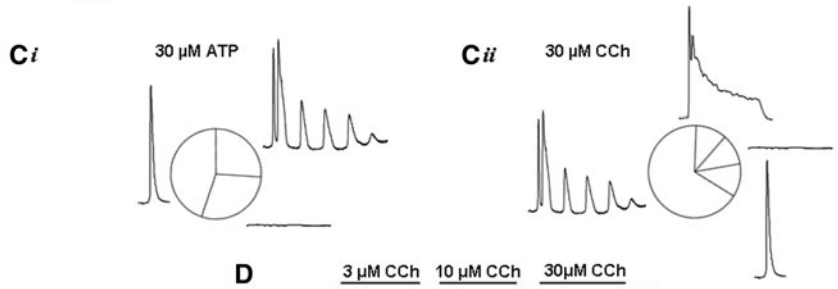

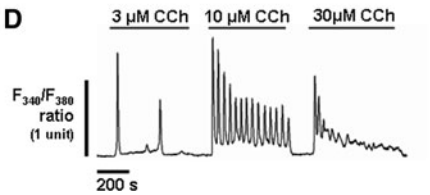

Fig. 1 Assessment of the temporal patterns of dynamic agonist-evoked $[Ca^{2+}]_i$ responses in untransfected HEK293 cells. $[Ca^{2+}]_i$ responses (represented as fura-2 F340/F380 ratio) were measured in fura-2-loaded HEK293 cells in response to various agonists at endogenous receptors, including carbachol (CCh), ATP, histamine and bradykinin. **a** Representative trace showing $[Ca^{2+}]_i$ responses induced by 30 μM histamine (no response), 30 μM ATP (single transient $[Ca^{2+}]_i$ spike) or 30 μM CCh ($[Ca^{2+}]_i$ oscillations) on the same cell. **b** Table showing the proportion of cells exhibiting $[Ca^{2+}]_i$ response induced by ATP, CCh, histamine and bradykinin. **c** Pie charts indicate the proportion of cells that gave each type of response (no response, single peak, $[Ca^{2+}]_i$ oscillations, or sustained response) when exposed to either 30 μM ATP (**c-i**) or 30 μM CCh (**c-ii**). Types of response are indicated next to the segment of the pie chart that corresponds to the proportion of cells that exhibited that given response. **d** CCh evoked robust and reproducible, concentration-dependent frequency modulated $[Ca^{2+}]_i$ oscillations in HEK293 cells stably expressing the muscarinic M3 receptor (HEK293 M3). However, these cells could not be patch clamped when transfected with cDNA (see Results) as a result of difficulties in obtaining a seal and thus were not used as a model system in subsequent experiments

This was done to determine which agonists would produce the most reliable and consistent oscillatory $[Ca^{2+}]_i$ responses in the greatest number of cells. The majority of cells evoked a $[Ca^{2+}]_i$ response to carbachol and ATP (carbachol, 89% from 84 cells, $n = 19$; ATP, 68% from 87 cells, $n = 20$; Fig. 1a, b), while very few cells evoked any $[Ca^{2+}]_i$ response to histamine or bradykinin (histamine, 1% from 80 cells, $n = 18$; bradykinin, 6% from 36 cells, $n = 8$; Fig. 1a, b). However, cells that did respond to histamine evoked robust and repetitive $[Ca^{2+}]_i$ oscillations. Representative responses of untransfected HEK293 cells to agonists are shown in Fig. 1a, and the relative number of cells that responded are summarized in Fig. 1b. Responses to agonists were highly variable and heterogeneous. In an attempt to quantify this heterogeneity, responses were categorized into no response, a single spike, oscillations or a sustained response, and the number of cells exhibiting each response determined (Fig. 1c). A large proportion of cells exposed to 30 μM ATP produced a single peak (43% from 87 cells, $n = 20$; Fig. 1c-i), while the majority of cells exposed to 30 μM carbachol produced oscillations (67% from 84 cells, $n = 19$; Fig. 1c-ii). Therefore, in most experiments where dynamic changes in $[Ca^{2+}]_i$ were simultaneously measured with K_{Ca} channel activity, HEK293 cells were stimulated with 30 μM CCh because this produced robust, temporally distinct $[Ca^{2+}]_i$ oscillations in the largest proportion of cells. These data show that the use of untransfected HEK293 cells provide a suitable model system in which to study the effect of temporally distinct patterns of agonist-evoked $[Ca^{2+}]_i$ signals on K_{Ca} channel activity.

During initial experiments, the use of the HEK293 M3 cells (which stably express a muscarinic receptor, M3) appeared to be an ideal model for further studies because the temporal profile of CCh-evoked $[Ca^{2+}]_i$ signaling could be predictably manipulated by simply changing the concentration of CCh (see Fig. 1d and Yang et al. 1995). However, subsequent transfection with DNA encoding K_{Ca} channels made patch clamping difficult as a result of the inability to achieve a seal, which made HEK293 M3 cells unsuitable despite the reproducible $[Ca^{2+}]_i$ signals.

In addition, fura-2 imaging of agonist-evoked $[Ca^{2+}]_i$ signaling was performed on each stably expressing K_{Ca} cell line. Qualitatively, the temporal pattern of agonist-evoked

$[Ca^{2+}]_i$ signaling was indistinguishable from untransfected HEK293 cells.

Characterization of the Electrophysiological and Pharmacological Properties of K_{Ca}-Expressing HEK293 Cell Lines

Before we could test the effects of dynamic changes in $[Ca^{2+}]_i$ on K_{Ca} channel activity, it was important to confirm the functional expression of each K_{Ca} channel (small conductance (SK3), intermediate conductance (hIK1), or large conductance (BK_{STREX} splice variant) K_{Ca} channel) when stably expressed in HEK293 cells. This was achieved by recording whole-cell K^+ currents using a voltage step protocol (−100 mV to 110 mV, 10-mV increments, 100 ms per step, holding potential −60 mV) and with steady-state $[Ca^{2+}]$ set at either 100 nM or 3 μM in the patch pipette. These concentrations were chosen because 100 nM Ca^{2+} represents resting $[Ca^{2+}]_i$ and thus K_{Ca} activity under resting conditions. Likewise, 3 μM Ca^{2+} was chosen as this represents typically high $[Ca^{2+}]_i$ achieved during stimulation, whereby K_{Ca} channels might be expected to be maximally activated. Each stable cell line exhibited biophysical and pharmacological properties characteristic of each respective recombinantly expressed channel, is summarized in Figs. 2, 3, and 4, and is qualitatively similar to previous reports (Barfod et al. 2001; Grunnet et al. 2001).

Untransfected HEK293 cells exhibited a negligible endogenous K^+ current (4 ± 1 pA/pF at +40 mV; $n = 8$), which was significantly smaller than the current exhibited by HEK293 SK3 cells (68 ± 13 pA/pF; $n = 13$; $P \leq 0.01$; Fig. 2a, c, d), HEK293 hIK1 cells (32 ± 3 pA/pF; $n = 23$; $P \leq 0.001$; Fig. 4a, c), or HEK293 BK cells (19 ± 6 pA/pF; $n = 10$; $P \leq 0.05$; Fig. 4b, d). Moreover, these endogenous currents in untransfected HEK293 cells were unaffected by the SK opener riluzole (3 ± 0.3 pA/pF, $n = 8$) or by the SK blocker apamin (9 ± 1 pA/pF, $n = 5$). This indicated that any endogenous K^+ current present in K_{Ca}-expressing HEK293 cells was unlikely to contribute significantly to the size of the K_{Ca} current observed.

HEK293 SK3 cells exhibited "SK-like" K^+ currents that were activated by high Ca^{2+} (3 μM, 68 ± 13 pA/pF;

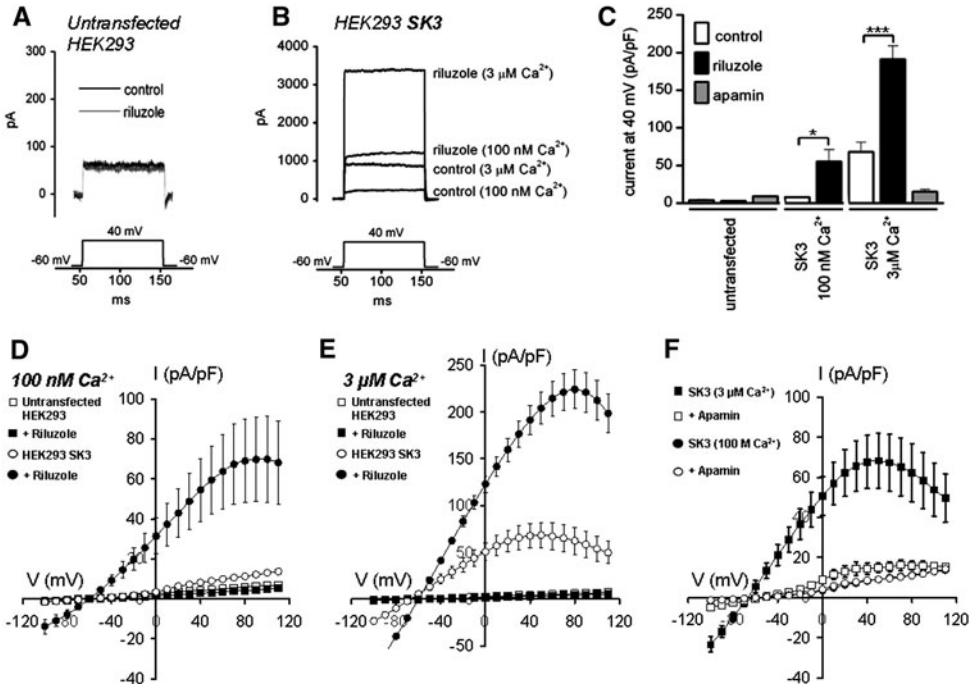

Fig. 2 Whole-cell current recordings and pharmacological characterization of HEK293 SK3 cells. The whole-cell patch clamp technique in the voltage clamp mode was used to evaluate whole-cell currents in HEK293 SK3 cells. Raw voltage clamp current–voltage (I/V) trace showing the current at +40 mV (holding potential −60 mV) in untransfected HEK293 cells (**a**) and HEK293 SK3 cells (**b**) with or without the SK opener, riluzole. **c** Comparison of the average current at +40 mV in the presence and absence (*white bars*) of 300 μM riluzole (*black bars*) or 100 nM apamin (*gray bars*), for untransfected HEK293 cells and HEK293 SK3 cells with $[Ca^{2+}]_i$ set at 100 nM or 3 μM. (* $P < 0.05$, *** $P < 0.001$). **d** Mean I/V relationship for HEK293 SK3 cells with pipette solutions containing 100 nM $[Ca^{2+}]_i$; untransfected HEK293 control (*open squares*), untransfected HEK293 and 300 μM riluzole (*closed squares*), HEK293 SK3 (*open circles*), HEK293 SK3 and 300 μM riluzole (*closed circles*). **e** Mean I/V relationship for HEK293 SK3 cells as in *D*, except pipette solutions contained 3 μM Ca^{2+}. *F.*, Mean I/V relationship for HEK293 SK3 cells as in (**d**) and (**e**), except pipette solutions contained 3 μM Ca^{2+} in the absence (*black box*) or presence of 100 nM apamin (*white box*); or pipette solutions contained 100 nM Ca^{2+} in the absence (*black circle*) or presence of 100 nM apamin (*white circle*)

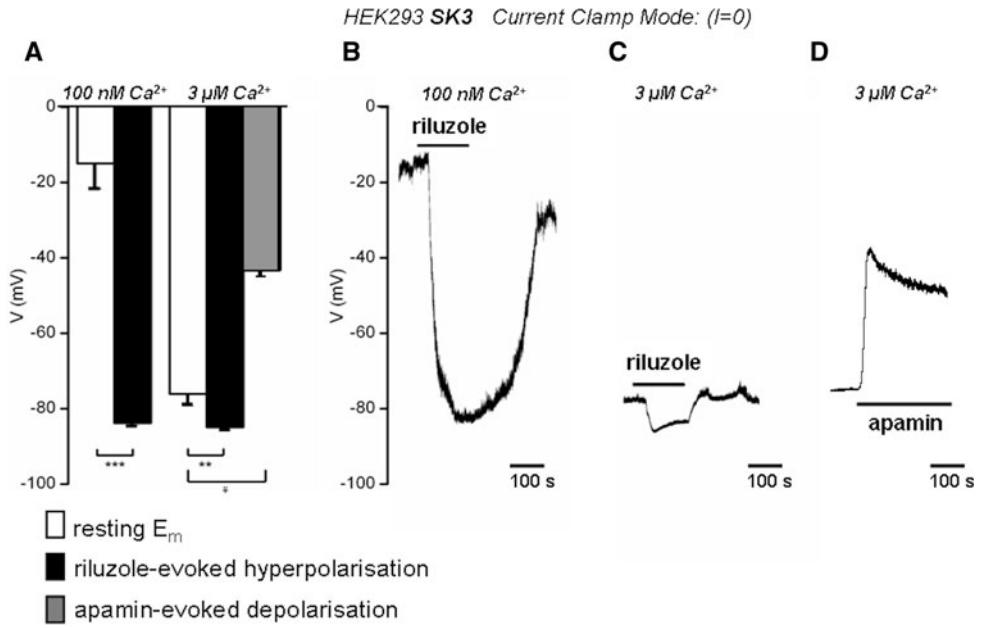

Fig. 3 Membrane potential recordings and pharmacological characterization of HEK293 SK3 cells. Membrane potential recordings were carried out using a current-clamp protocol where the current was clamped at zero in HEK293 SK3 cells in the absence and presence of the SK opener, riluzole, and SK inhibitor, apamin. Membrane potential was measured before, during and after application of drug. **a** Comparison of average resting membrane potential (V) at rest and before application of drug (*white bars*) and during riluzole-evoked hyperpolarization (*black bars*) and during apamin-evoked depolarization (*gray bar*) with pipette solution containing either 100 nM (**b**) or 3 µM free Ca^{2+} (**c**, **d**). * $P < 0.05$; ** $P < 0.01$ (Wilcoxon signed rank test), *** ($P < 0.0001$; paired *t*-test). **b**, **c**, **d** Representative membrane potential recording showing the effect of application of 300 µM riluzole, with the pipette solution contained either 100 nM free Ca^{2+} (**b**) or 3 µM free Ca^{2+}(**c**) or the effect of apamin with the pipette solution containing 100 nM free Ca^{2+} (**d**)

$n = 13$), compared to low free Ca^{2+} (100 nM, 8 ± 0.5 pA/pF, $n = 5$; $P \leq 0.05$; Fig. 2b–d), with a reversible potential of −60 mV and a peak current at +50 mV. These K^+ currents were also markedly potentiated by the SK opener riluzole (300 µM) when measured at both 100 nM (55 ± 16 pA/pF, $n = 5$; Fig. 2b–d) and 3 µM free Ca^{2+} (191 ± 18 pA/pF, $n = 5$; Fig. 2b, c, e; $P \leq 0.001$). Moreover, K^+ currents in HEK293 SK3 cells were also inhibited by the SK inhibitor apamin (100 nM), at 3 µM free Ca^{2+} (14 ± 3 pA/pF, $n = 3$; Fig. 2c, f; $P \leq 0.001$). Riluzole had no effect on current amplitudes at +40 mV in untransfected HEK293 cells (3 ± 0.3 pA/pF, $n = 8$, Fig. 2a, c) compared to untreated cells (4 ± 1 pA/pF, $n = 8$; Fig. 2a, c), demonstrating that riluzole was unlikely to be exerting an effect on endogenous K^+ currents. Riluzole also caused a reversible hyperpolarization of the membrane potential to approximately −86 mV from a resting membrane potential of either −20 ± 7 mV at 100 nM free Ca^{2+} ($n = 5$, Fig. 3a, b) or −78 ± 3 mV at 3 µM free Ca^{2+} ($n = 10$, Fig. 3a, c, $P \leq 0.001$). Moreover, the SK blocker apamin caused a marked depolarization from the hyperpolarized resting membrane potential of −78 ± 3 mV (3 µM pipette Ca^{2+}) to −43 ± 2 mV ($n = 3$, Fig. 3a, d). These data therefore confirm the functional expression of SK3 currents in the HEK293 SK3 stable cell line.

Currents in HEK293 hIK1 and HEK293 BK cells were similarly characterized using the whole-cell patch clamp technique. In both cell types, K^+ currents were measured with free pipette [Ca^{2+}] set to 3 µM, again to mimic maximal Ca^{2+}-dependent activation of the K_{Ca} channels. In HEK293 hIK1 cells, an outward current characteristic of IK, with a reversal potential of −60 mV and a peak current amplitude of 35 ± 4 pA/pF at +70 mV ($n = 23$; Fig. 4a), was observed. The current–voltage relationship had a negative slope at potentials greater than +70 mV. Peak current amplitude was inhibited by 78% by 10 µM TRAM-34 to 6 ±2 pA/pF ($n = 5$; $P \leq 0.01$; Fig. 4a, c) and was increased 60% by 100 µM EBIO to 55 ± 7 pA/pF ($n = 8$; $P \leq 0.01$; Fig. 4a, c). Both 10 µM TRAM-34 ($n = 5$) and 100 µM EBIO ($n = 8$) had no significant effect when applied to untransfected HEK293 cells ($P > 0.05$; Fig. 4c). HEK293 BK cells exhibited a large outward current typical of BK channels (Fig. 4b, d). Current amplitudes at +80 mV (116 ± 19 pA/pF, $n = 10$; Fig. 4b, d) were inhibited 63% by 100 nM iberiotoxin to 44 ± 7 pA/pF ($n = 5$; $P \leq 0.05$; Fig. 4b, d). Application of 30 µM NS1619 enhanced current amplitudes at +80 mV by 171% to 315 ± 34 pA/pF ($n = 5$; $P \leq 0.001$; Fig. 4b, d). Both 100 nM iberiotoxin and 30 µM NS1619 had no significant effect on current amplitudes when applied to untransfected HEK293 cells ($n = 5$; $P > 0.05$; Fig. 4d).

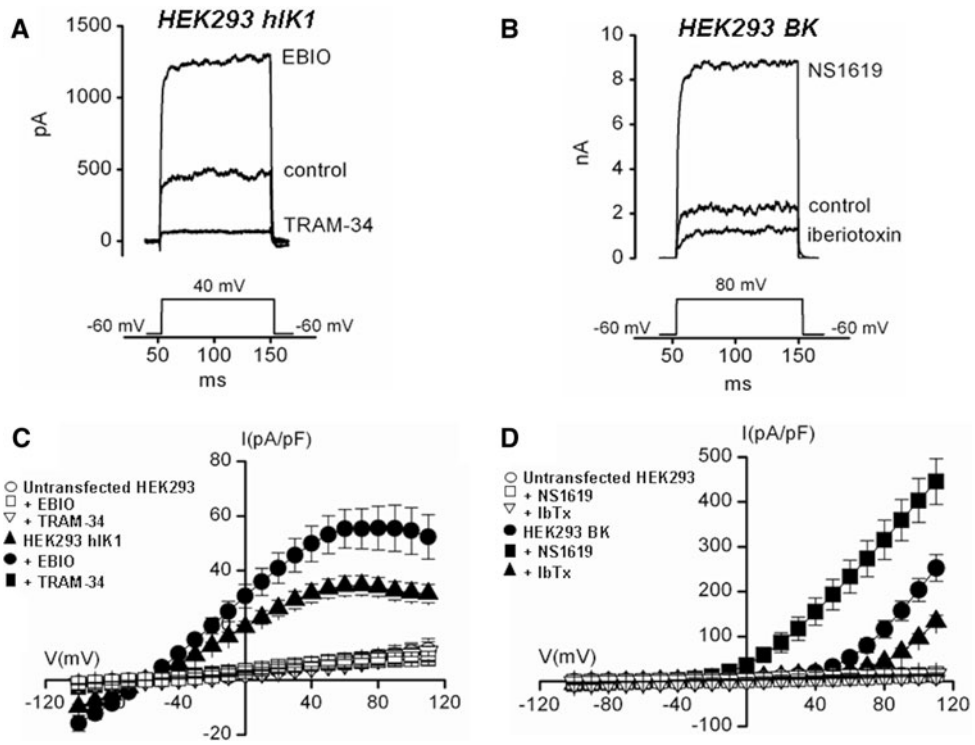

Fig. 4 Pharmacological characterization of HEK293 hIK1 and HEK293 BK cells. The whole-cell patch clamp technique was used to characterize HEK293 hIK1 (**a**, **d**) and HEK293 BK cells (**b**, **d**). Intracellular solutions contained 3 μM free Ca^{2+}. **a** Raw voltage clamp current–voltage (I/V) trace showing the IK-like current at +40 mV (**a**) and the BK-like current at +80 mV (**b**) from a holding potential of −60 mV. **c**, **d** Mean I/V relationship showing the effects of 10 μM TRAM-34 (*closed squares*) and 100 μM EBIO (*closed circles*) on whole-cell current in HEK293 hIK1 cells and **c** 100 nM iberiotoxin (IbTx) (*closed triangles*) and 30 μM NS1619 (*closed squares*) on whole-cell current in HEK293 BK cells (**c**)

Collectively, these results showed that HEK293 SK3, HEK293 hIK1, and HEK293 BK cell lines exhibited electrophysiological and pharmacological properties characteristic of SK, IK, and BK currents, respectively. These data are qualitatively similar to previous studies using recombinantly expressed K_{Ca} cell lines (Barfod et al. 2001; Chen et al. 2005; Erxleben et al. 2002; Gribkoff et al. 1996; Grunnet et al. 2001; Ishii et al. 1997; Jensen et al. 1998; Jiang et al. 2004b; Joiner et al. 1997; Logsdon et al. 1997; McCartney et al. 2005; Shipston et al. 1999; Wulff et al. 2000) and therefore represent suitable model systems in which to evaluate the effects of dynamic changes in $[Ca^{2+}]$ on K_{Ca} channel activity.

Effect of Dynamic $[Ca^{2+}]_i$ Changes on Membrane Potential in HEK293 SK3 Cells

Initial experiments simultaneously recorded $[Ca^{2+}]_i$ and membrane potential as an indicator of K_{Ca} channel activity, whereby 30 μM carbachol was applied to HEK293 SK3 cells to elicit $[Ca^{2+}]_i$ oscillation (Fig. 4). In this example, the carbachol-induced $[Ca^{2+}]_i$ oscillations were mirrored by the simultaneous hyperpolarization of the membrane potential. However, it was frequently found when recording membrane potential that the cells were unable to hyperpolarize beyond −74 mV, giving an apparent flattening of the trace (Fig. 4, expanded trace). This was likely due to the membrane potential approaching the equilibrium potential for K^+ for our experimental conditions. This made interpretation of experiments difficult; therefore, experiments we performed subsequently recorded membrane current instead of membrane potential as an indicator of K_{Ca} channel activity.

It was also noticed that during CCh treatment and in between successive $[Ca^{2+}]_i$ oscillations, there was a depolarizing drift in the baseline membrane potential (from approximately −30 mM to −5 mM in Fig. 4). On average, this CCh-induced depolarization of the baseline was found to be 20.5 ± 4.5 mV ($n = 13$). However, this slow drifting depolarization of the baseline seemed to occur independently of the oscillations in membrane potential that appeared to mirror the oscillations in $[Ca^{2+}]_i$. This therefore suggests that this contaminating conductance may be Ca^{2+} independent, or at least occurs independent of dynamic $[Ca^{2+}]_i$ changes. This suggests that CCh may activate an endogenous, depolarizing current in HEK293 cells, such as a nonselective cation channel (e.g., TRP channel), or Ca^{2+}-activated Cl^- current, or inhibit a background K^+ channel. Similarly, ionomycin has also been shown to induce a depolarizing drift in untransfected HEK293 cells, most likely due to a Ca^{2+}-dependent conductance (Saleem et al. 2009). However, the CCh-evoked depolarization in the current study may be Ca^{2+} independent, for example as a result of a DAG-induced activation of TRPC channels (Hardie 2007; Soboloff et al. 2007). The full characterization of this endogenous depolarizing conductance in HEK293 cells, although intrinsically interesting, is beyond the scope of the current study.

CCh-evoked Dynamic $[Ca^{2+}]_i$ Signals Generated Heterogeneous K_{Ca} Current Responses

For technical reasons, not every cell in which $[Ca^{2+}]_i$ and K_{Ca} currents were simultaneously measured could be calibrated. Therefore, the uncalibrated indo-1 405/485 ratio was used to represent changes in $[Ca^{2+}]_i$ in all traces (Figs. 5, 6, 7, 8, 10). However, periodic calibrations were carried out in each cell line to estimate the $[Ca^{2+}]_i$ (depicted in the relevant traces shown in Figs. 7, 10). Baseline $[Ca^{2+}]_i$ levels before the experiment was commenced were estimated to be 55 ± 4 nM (SK3 HEK293, $n = 11$), 88 ± 10 nM (IK1 HEK293, $n = 10$) and 68 ± 9 nM (SK3 HEK293, $n = 15$). On average, the peak CCh-evoked $[Ca^{2+}]_i$ response was estimated to be 886 ± 276 nM (SK3 HEK293, $n = 11$), 597 ± 235 nM (IK1 HEK293, $n = 10$), and 503 ± 47 nM (BK HEK293, $n = 15$). The relationship between dynamic changes in $[Ca^{2+}]_i$ evoked by Ca^{2+}-mobilizing agonists and K_{Ca} channel activity was complex and varied, resulting in a large degree of heterogeneity. Categorizing responses and counting the number of cells that showed each type of response helped to quantify this heterogeneity.

Because local $[Ca^{2+}]_i$ signals are sufficient to activate K_{Ca} channels, it was necessary to identify the size of change in global $[Ca^{2+}]_i$ that was likely to approximate to a local $[Ca^{2+}]_i$ signal. Preliminary imaging experiments in primary cultured ECs revealed that on average, localized

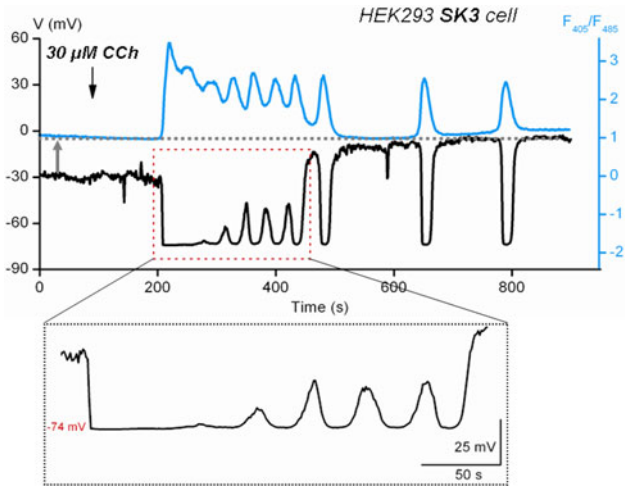

Fig. 5 Representative example of a simultaneous $[Ca^{2+}]_i$ and membrane potential recording (V) in response to 30 μM carbachol. HEK293 SK3 cells were loaded with 2.5 μM indo-1 AM to monitor $[Ca^{2+}]_i$ (*blue* or *gray*). The membrane potential (*black*) was measured simultaneously, in response to 30 μM carbachol (*see arrow*) in current-clamp mode using the perforated patch clamp method. The trace in the dotted box is enlarged in the lower panel and shows that the equilibrium potential for K^+ under the experimental conditions did not allow for hyperpolarization beyond −74 mV, which caused the trace to flatten. (Color figure online)

$[Ca^{2+}]_i$ signals (e.g., Ca^{2+} puffs) represented 3–5% of the maximum global $[Ca^{2+}]_i$ signal when measured across the entire cell. Therefore, a $[Ca^{2+}]_i$ peak was defined as a F_{405}/F_{485} change of ≥ 0.1 ratio units (∼ 40 nM estimated change in $[Ca^{2+}]_i$) because this value represented approximately 3% of the maximum global $[Ca^{2+}]_i$ response when measured across the entire cell using fura-2 imaging techniques. To distinguish a current peak from noise, the average noise for each trace was calculated, and a change of ≥ 50 pA was considered to be a real current peak because this value was two standard deviations away from the average noise. A current peak and $[Ca^{2+}]_i$ peak was said to occur simultaneously if the apex of the current peak occurred within 1 s of the apex of the $[Ca^{2+}]_i$ peak.

The responses were categorized into five response types, as follows. (1) The current faithfully followed the shape of the $[Ca^{2+}]_i$ response (Fig. 5), where the percentage of $[Ca^{2+}]_i$ and current peaks that occurred simultaneously within a trace was ≥ 85%. (2) The response exhibited current-independent $[Ca^{2+}]_i$ events (where some $[Ca^{2+}]_i$ peaks did not evoke current peaks). This represented a disconnection between an increase in $[Ca^{2+}]_i$ and activation of K_{Ca} currents. (3) The resposne exhibited Ca^{2+}-independent current events (where some current peaks occurred in the absence of a noticeable change in $[Ca^{2+}]_i$). (4) The response exhibited Ca^{2+}-independent current events (as above), which corresponded to subthreshold changes in $[Ca^{2+}]_i$ (< 40 nM) that were not large enough to be categorized as $[Ca^{2+}]_i$ peaks but were noticeable on the $[Ca^{2+}]_i$ trace (Ca^{2+} blips). Such Ca^{2+} blips may conceivably represent local changes in $[Ca^{2+}]_i$ and were therefore included as a subcategory during analysis. (5) The response exhibited a response that displayed both current-independent Ca^{2+} events and Ca^{2+}-independent current events.

The total number of individual $[Ca^{2+}]_i$ peaks (≥ 0.1 ratio units, or 40 nM Ca^{2+}) per trace, individual current peaks (≥ 50 pA) per trace, and the number of $[Ca^{2+}]_i$ and current peaks that occurred simultaneously per trace were counted. From this, the number of Ca^{2+}-independent current events per trace was determined and expressed as a percentage of the total number of current events. Likewise, the number of current-independent $[Ca^{2+}]_i$ events per trace was determined and expressed as a percentage of the total number of $[Ca^{2+}]_i$ events. This analysis was performed for each K_{Ca} subtype.

Figure 6 exemplifies how the agonist-evoked $[Ca^{2+}]_i$ oscillations induced a K_{Ca} current (in this case, hIK1 current) that simultaneously followed the pattern of $[Ca^{2+}]_i$ signal. Although in some cells there appeared to be a general correlation between $[Ca^{2+}]_i$ peaks and current peaks, in many cells, current-independent $[Ca^{2+}]_i$ events and/or Ca^{2+}-independent current events were frequently

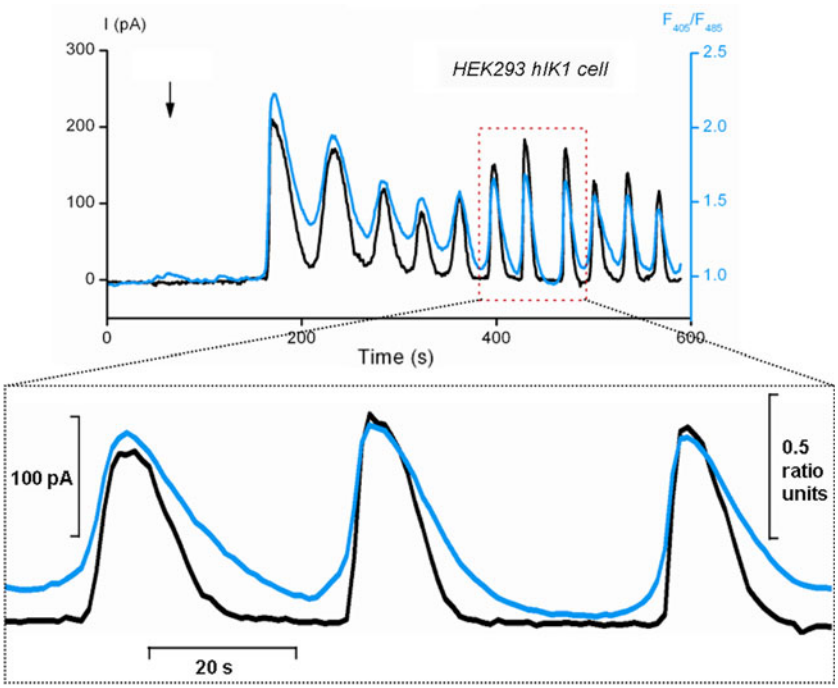

Fig. 6 Simultaneous $[Ca^{2+}]_i$ and K_{Ca} current recording showing a typical example of how the K_{Ca} current can faithfully follow the agonist-evoked $[Ca^{2+}]_i$ signal. HEK293 hIK1 cells were loaded with 2.5 μM indo-1 AM to monitor $[Ca^{2+}]_i$ (*blue* or *gray*). The membrane current was measured simultaneously, in response to the 10 μM histamine (*arrow*) using the perforated patch clamp method. The trace in the dotted box is enlarged and the $[Ca^{2+}]_i$ trace normalized to the current trace (*lower panel*) and further illustrates that the $[Ca^{2+}]_i$ and current (*black*) oscillations were synchronized. (Color figure online)

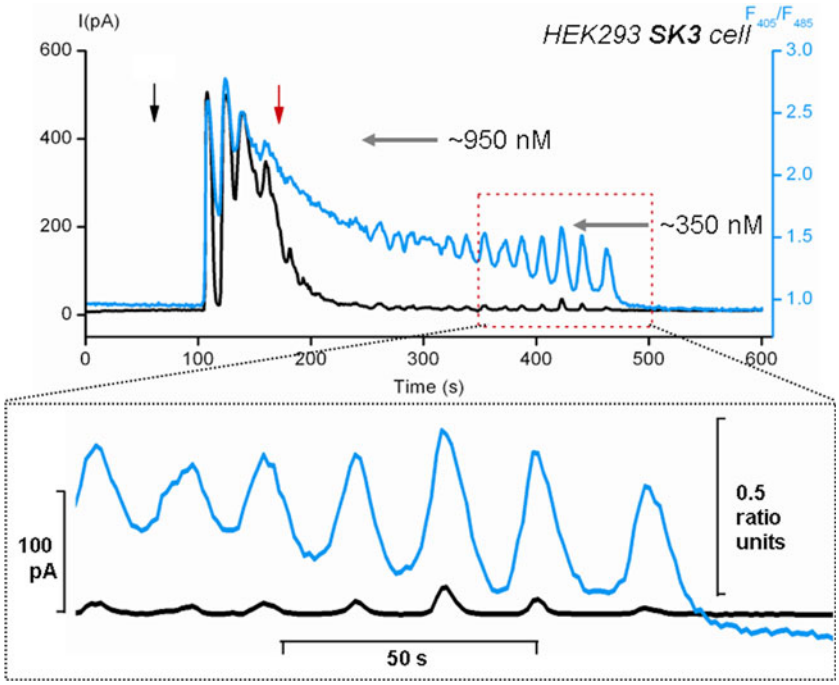

Fig. 7 Simultaneous $[Ca^{2+}]_i$ and K_{Ca} recording showing a typical example of current independent $[Ca^{2+}]_i$ events. HEK293 SK3 cells were loaded with 2.5 μM indo-1 AM to monitor $[Ca^{2+}]_i$ (depicted as indo-1 F405/F485 ratio, *blue* or *gray*). The membrane current was measured simultaneously, in response to 30 μM carbachol (*arrow*), using the perforated patch clamp method. The *red arrow* indicates the point at which there appears to be a disconnection between $[Ca^{2+}]_i$ and K_{Ca} current occurred. The trace in the dotted box is enlarged in the *lower panel* and shows that there were oscillations in $[Ca^{2+}]_i$ (*blue* or *gray*) that did not evoke substantial changes in K_{Ca} current (*black*). The estimated $[Ca^{2+}]_i$ (nM), as assessed from periodic in situ calibration experiments, is indicated at the side of the *arrows*. (Color figure online)

observed (Figs. 7, 8, 10). Moreover, these events were observed to varying degrees in different K_{Ca}-expressing HEK293 cell lines (Fig. 11).

In some cells (i.e., at the point indicated by the red arrow in Fig. 7), there appeared to be a disconnection between $[Ca^{2+}]_i$ and K_{Ca} current, whereby the current declined

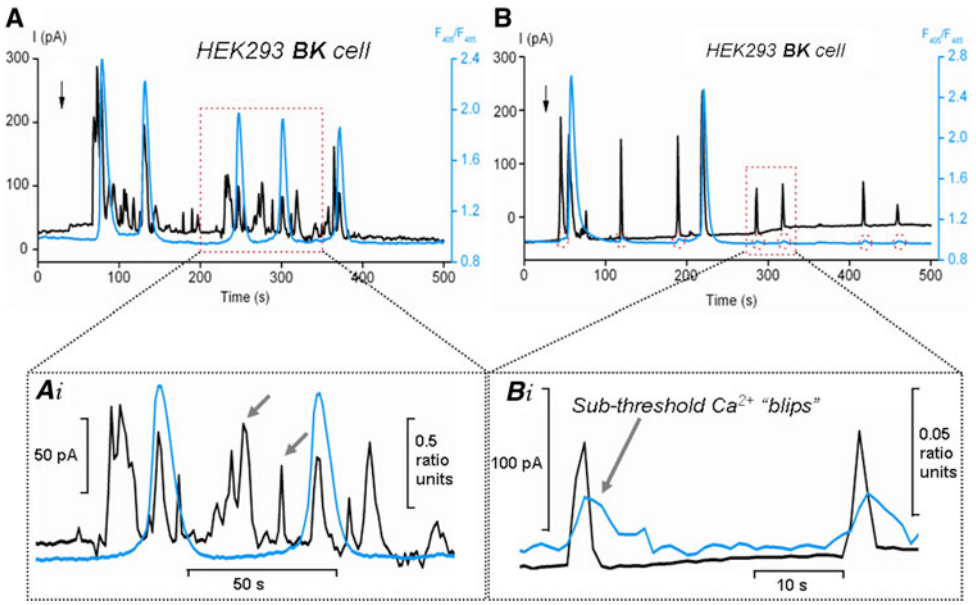

Fig. 8 Simultaneous $[Ca^{2+}]_i$ and K_{Ca} current recordings showing typical examples of Ca^{2+}-independent current events. HEK293 BK cells were loaded with 2.5 μM indo-1 AM to monitor $[Ca^{2+}]_i$ (depicted as indo-1 F405/F485 ratio, *blue* or *gray*). The membrane current was measured simultaneously, in response to 30 μM carbachol (*arrow*), using the perforated patch clamp method. The trace in the dotted red box is enlarged in (**a-i**) and shows that there were changes in current (*black*) independent of any change in $[Ca^{2+}]_i$ (*blue* or *gray*). **b** Simultaneous $[Ca^{2+}]_i$ and K_{Ca} recordings showing a typical example of a cell exhibiting Ca^{2+}-independent current events that corresponded to tiny $[Ca^{2+}]_i$ blips The dotted circles indicate tiny blips in $[Ca^{2+}]_i$ that were too small to register as a global $[Ca^{2+}]_i$ peak, but may be attributable to local Ca^{2+} release events. The trace in the *dotted box* is enlarged in the *lower panel* of (**b-i**) and shows that the tiny blips in $[Ca^{2+}]_i$ evoked substantial changes in K_{Ca} current. (Color figure online)

much faster than the $[Ca^{2+}]_i$. Expansion of another segment of the trace, as indicated by the red box (Fig. 7), demonstrates a series of $[Ca^{2+}]_i$ peaks that did not evoke a significant change in current, termed current-independent $[Ca^{2+}]_i$ events. Both of these phenomena may be due to some kind of time-dependent or Ca^{2+}-dependent rundown or inhibition of the K_{Ca} current—that is, where the same magnitude $[Ca^{2+}]_i$ peak that had previously activated a robust K_{Ca} current failed to activate or activated a severely diminished current in the same trace. A similar example is also shown in Fig. 10 for HEK293 BK cells. Further, although each $[Ca^{2+}]_i$ peak in Fig. 8 (HEK293 BK) was accompanied by a corresponding current peak, there were a substantial number of additional current peaks that occurred independently of any change in $[Ca^{2+}]_i$, termed Ca^{2+}-independent current events (enlarged in Fig. 8a). It is important to note that some of these Ca^{2+}-*independent* current events were of a similar size to Ca^{2+}-*dependent* current events, further supporting the presence of some kind of desynchronization of $[Ca^{2+}]_i$ and K_{Ca} current.

In some cases of Ca^{2+}-independent current events, it appeared that the current peaks corresponded to very small changes in $[Ca^{2+}]_i$ that were below the threshold (0.1 change in ratio, ~40 nM change in $[Ca^{2+}]_i$) to be recorded as a bona fide $[Ca^{2+}]_i$ peak, but still visible on the trace (subthreshold Ca^{2+} blips). For example, each tiny change in $[Ca^{2+}]_i$ (indicated by the dotted circles in Fig. 8b) was accompanied by a current peak. The experiments performed only measured the average changes in $[Ca^{2+}]_i$ over the entire single patch clamped cell, using a photomultiplier-based detection system. Therefore, any local $[Ca^{2+}]_i$ signals may have been too small to be detected or may have been detected as subthreshold Ca^{2+} blips in the average $[Ca^{2+}]_i$ over the entire cell, as seen in Fig. 8b and enlarged in Fig. 8b-i. It is well known that BK channels in particular can be activated by local increases in $[Ca^{2+}]_i$ within microdomains to produce spontaneous transient outward currents (Nelson et al. 1995; Zhuge et al. 2002); therefore, this could be a similar phenomenon. For technical reasons, it was not possible to measure localized $[Ca^{2+}]_i$ signals simultaneously with K_{Ca} currents. However, when agonist-evoked $[Ca^{2+}]_i$ signaling was measured in each K_{Ca}-expressing HEK293 cell line during parallel fura-2-imaging experiments, localized $[Ca^{2+}]_i$ signals were never observed, but rather global oscillating $[Ca^{2+}]_i$ waves were observed. An example of this is shown in Fig. 9 in HEK293 BK cells, whereby CCh evoked an increase in $[Ca^{2+}]_i$ that initiated within one specific region of the cell (indicated by the blue box in image A and blue trace in Fig. 9) and then slowly propagated to the opposite side of the cell (indicated by the red box in image A and red trace in Fig. 9). This leads to $[Ca^{2+}]_i$ oscillations that occur

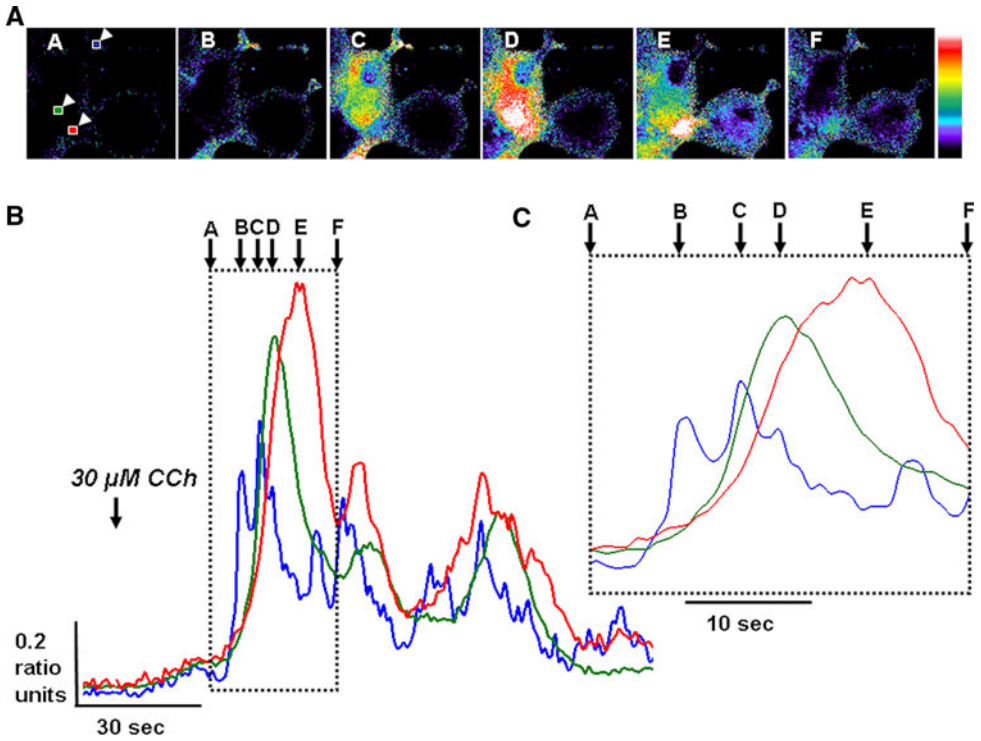

Fig. 9 Carbachol-evoked spatial and temporally distinct $[Ca^{2+}]_i$ waves in HEK293 BK cells. The spatial and temporal properties of agonist-evoked $[Ca^{2+}]_i$ signals were assessed in all three K_{Ca}-expressing cell lines (HEK293 SK3, HEK293 IK, and HEK293 BK) using fura-2-imaging of intact (non-patch clamped) cells. The example shown here represents just one experiment (out of four), whereby HEK293 BK cells exhibited such complex spatiotemporal $[Ca^{2+}]_i$ waves. In all other experiments, all cells exhibited rapid global $[Ca^{2+}]_i$ waves and localized $[Ca^{2+}]_i$ signals were never observed. **a** Series of pseudo-colored fura-2 ratiometric images (*A–F*) of HEK293 BK cells loaded with 3 μM fura-2 AM to track the spatiotemporal carbachol (CCh)-evoked $[Ca^{2+}]_i$ signals. **a–f** Images taken at the time points indicated in traces in (**b**) and (**c**). **b** Kinetic profile of CCh-evoked $[Ca^{2+}]_i$ waves that initiate in the projection-like region, depicted in (**a**) as a *blue box (blue trace)*, and propagates to the region depicted by the green box (*green trace*), and then finally to the region depicted by the red box (*red trace*). **c** Represents an expanded time scale of the trace within the dotted box in (**b**). (Color figure online)

slightly out of phase ($\sim$ 5 s) in different regions of the cell and, depending on the relative localization of K_{Ca} channels in the plasma membrane, may lead to a slight desynchronization between $[Ca^{2+}]_i$ and K_{Ca} currents. However, this is unlikely to account for all the Ca^{2+}-independent current events or current independent $[Ca^{2+}]_i$ events observed in the current study.

Comparison of the Relationship Between the Dynamic $[Ca^{2+}]_i$ Response and K_{Ca} Channel Activity Between SK3, hIK1, and BK-Expressing HEK293 Cells

The number of cells that evoked each of the five response type categories was determined for each K_{Ca}-expressing cell line (Fig. 11a). The main response type in HEK293 SK3 cells (Fig. 11a-i) was Ca^{2+}-independent current events (6 out of 11 cells; 55%), whereas 27% (3 out of 11 cells) showed a response where the current faithfully followed the $[Ca^{2+}]_i$ signal and 18% (2 out of 11 cells) exhibited current-independent $[Ca^{2+}]_i$ events. In HEK293 hIK1 cells, current faithfully followed the $[Ca^{2+}]_i$ signal in 50% (5 out of 10 cells), while the remaining 50% (5 out of 10 cells) exhibited Ca^{2+}-independent current events. Finally, HEK293 BK current faithfully followed the $[Ca^{2+}]_i$ signal in only 13% (2 out of 15 cells) of cells, with a further 13% (2 out of 15 cells) exhibiting both current-independent $[Ca^{2+}]_i$ events and Ca^{2+}-independent current events, 20% (3 out of 15 cells) displaying current-independent $[Ca^{2+}]_i$ events, while 53% (8 out of 15 cells) produced Ca^{2+}-independent current events. Of these, three out of the eight cells exhibited subthreshold changes in $[Ca^{2+}]_i$, possibly attributable to local Ca^{2+} release.

To allow more detailed analysis of each K_{Ca} subtype and to further quantify the degree of $[Ca^{2+}]_i$-current synchronization, the total number of individual $[Ca^{2+}]_i$ peaks and individual current peaks were counted in each trace and the average number of agonist-evoked Ca^{2+}-independent current events per trace was expressed as a percentage of the total number of current events (Fig. 11b). Likewise, the average number of current-independent $[Ca^{2+}]_i$ events per trace was expressed as a percentage of the total number of $[Ca^{2+}]_i$ events (Fig. 11c). This represented the extent by which there was a disconnection between an increase in $[Ca^{2+}]_i$ (Ca^{2+} spike) and the activation of K_{Ca} currents.

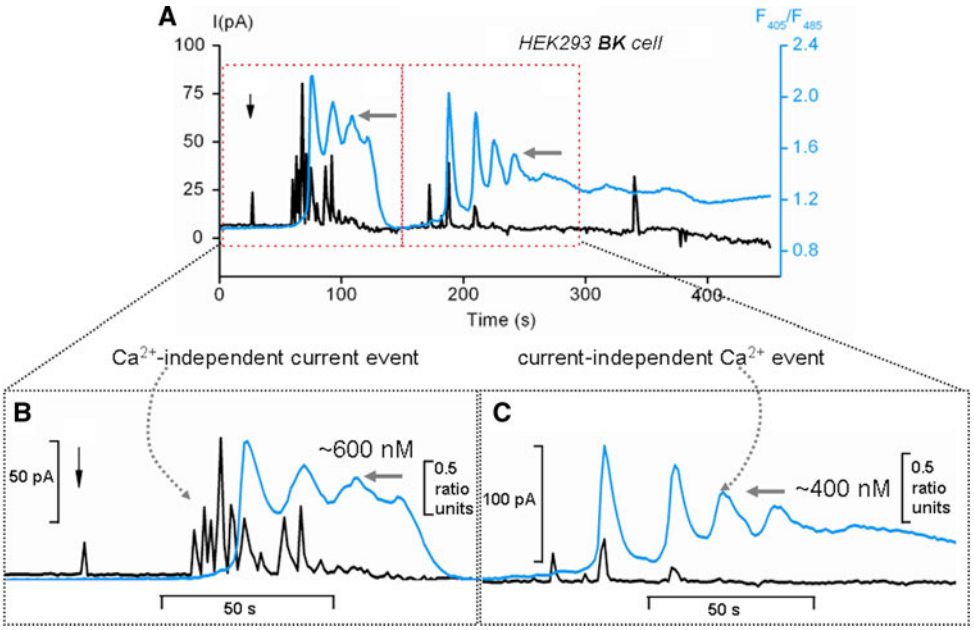

Fig. 10 Simultaneous $[Ca^{2+}]_i$ and K_{Ca} current recordings showing typical examples of both Ca^{2+}-independent current events and current-independent $[Ca^{2+}]_i$ events. HEK293 BK cells were loaded with 2.5 μM indo-1 AM to monitor intracellular $[Ca^{2+}]_i$ (depicted as indo-1 F405/F485 ratio, *blue* or *gray*). (**a**) The membrane current was measured simultaneously in response to 30 μM carbachol (*arrow*), using the perforated patch clamp method. The traces in the dotted boxes in (**a**) are enlarged in (**b**) and (**c**) (separate scales), showing that there were both Ca^{2+}-independent current events (**b**) and current-independent $[Ca^{2+}]_i$ events (**c**), respectively. In these examples, $[Ca^{2+}]_i$ and K_{Ca} current appear completely unsynchronized. The estimated $[Ca^{2+}]_i$ (nM), as assessed from periodic in situ calibration experiments, is indicated at the side of the *arrows*. (Color figure online)

Analyzing the data in this way takes into account variability in the frequency of $[Ca^{2+}]_i$ or current peaks between experiments and allows for comparison between K_{Ca} subtypes.

The number of cells in which Ca^{2+}-independent current events were observed was approximately 50% for all three K_{Ca} channel subtypes (Fig. 11a). However, there were differences in the frequency with which these events occurred between K_{Ca} subtypes (Fig. 11b). Ca^{2+}-independent current events occurred least frequently in HEK293 SK3 cells, in which approximately 24% of all current events occurred without a corresponding increase in $[Ca^{2+}]_i$ (Ca^{2+} spike). This was significantly greater in HEK293 BK cells, whereby 50% of all current events were independent of an increase in $[Ca^{2+}]_i$ ($P \leq 0.05$). Ca^{2+}-independent current events represented 44% of all current events in HEK293 hIK1 cells (Fig. 11b). It is possible that some of the Ca^{2+}-independent current events may not be true Ca^{2+}-independent current events because the system used in this study to monitor $[Ca^{2+}]_i$ was only capable of detecting total $[Ca^{2+}]_i$ averaged over the entire cell and thus unable to detect local changes in $[Ca^{2+}]_i$. However, as stated previously, localized $[Ca^{2+}]_i$ signals were never observed in any K_{Ca}-expressing HEK293 cell using fura-2 imaging, although we cannot completely rule out such phenomena when cells are patch clamped using the perforated patch technique.

Changes in $[Ca^{2+}]_i$ (Ca^{2+} spikes) that occurred without a corresponding current spike most likely represented a true disconnection between an increase in $[Ca^{2+}]_i$ and activation of K_{Ca} currents. These current-independent $[Ca^{2+}]_i$ events also occurred most frequently in HEK293 BK cells, in which 36% of all $[Ca^{2+}]_i$ peaks did not evoke a change in current. This was statistically greater than that for HEK293 hIK1 cells ($P \leq 0.05$). Almost all $[Ca^{2+}]_i$ spikes elicited a corresponding change in current spike in both HEK293 hIK1 cells and HEK293 SK3 cells. There were almost no current-independent $[Ca^{2+}]_i$ events in HEK293 hIK1 cells (2%, Fig. 9c), with slightly more in HEK293 SK3 cells (15%, Fig. 9c). $[Ca^{2+}]_i$ spikes without a corresponding current spike could have occurred because the $[Ca^{2+}]_i$ spikes failed to reach the threshold for activation of the corresponding K_{Ca} current. By means of conventional whole-cell patch clamping, where Ca^{2+} is buffered to steady state, the Ca^{2+} sensitivities (EC_{50}) have been reported to be ~100–300 nM for IK (Ishii et al. 1997; Joiner et al. 1997; Logsdon et al. 1997), 600–700 nM for SK (Barfod et al. 2001; Xia et al. 1998), and > 1 μM for BK (Ahring et al. 1997; Erxleben et al. 2002; Petrik and Brenner 2007). However, the STREX splice variant of BK has been reported to have a higher sensitivity for Ca^{2+} at more negative potentials (Chen et al. 2005). Nevertheless, this could explain why current-independent $[Ca^{2+}]_i$ events

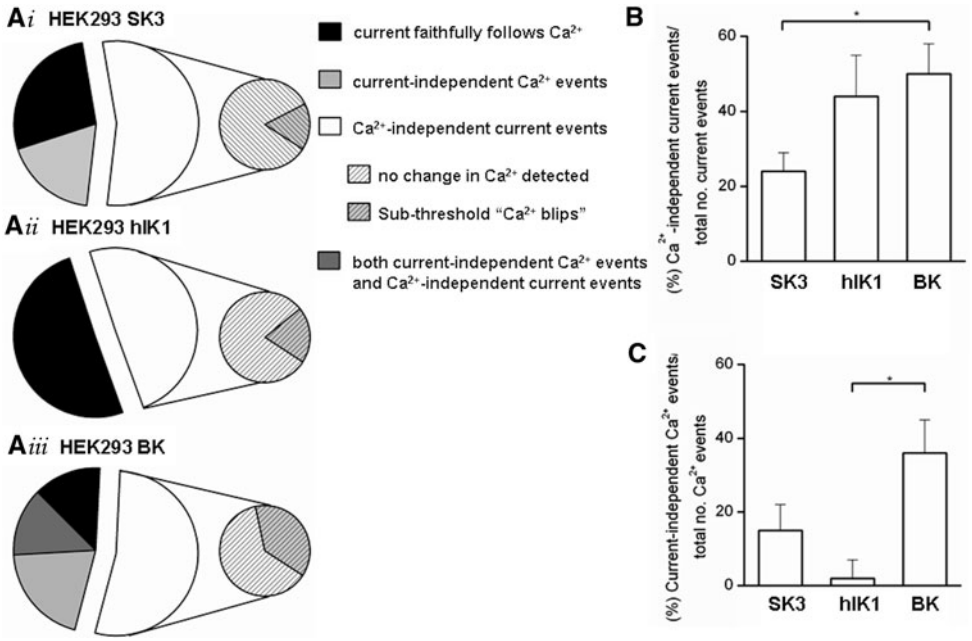

Fig. 11 Quantification of the heterogeneity of agonist-evoked $[Ca^{2+}]_i$ and K_{Ca} current responses for SK3, IK1, and BK-expressing HEK293 cells. $[Ca^{2+}]_i$ and K_{Ca} current were measured simultaneously in response to application of the agonist and the response type was categorized for HEK293 SK3 cells (**a-i,** $n = 11$), HEK293 hIK1 cells (**a-ii**, $n = 11$) and HEK293 BK cells (**a-iii**, $n = 15$). The smaller pie chart represents the proportion of cells from the Ca^{2+}-independent current events category that were further subcategorized where there was no detectable change in $[Ca^{2+}]_i$, or where there were tiny blips in $[Ca^{2+}]_i$ detected. **b** Comparison of the percentage of Ca^{2+}-independent current events between HEK293 SK3, HEK293 hIK1 and HEK293 BK cells. Mean percentage of the number of agonist-evoked Ca^{2+}-independent current events per trace/total number of current events per trace. **c** Comparison of the percentage of the current-independent $[Ca^{2+}]_i$ events between HEK293 SK3, HEK293 hIK1, and HEK293 BK cells. Mean percentage of the number of current-independent $[Ca^{2+}]_i$ events per trace/total number of $[Ca^{2+}]_i$ events per trace (* $P \leq 0.05$)

occurred more frequently in HEK293 BK cells than in either HEK293 SK3 or hIK1 cells.

This was even more apparent during high-frequency $[Ca^{2+}]_i$ oscillations or when oscillations fused into a sustained increase in $[Ca^{2+}]_i$, as shown in Fig. 7 in HEK293 SK3 cells. In this example, estimations of $[Ca^{2+}]_i$ from in situ calibrations reveal that the $[Ca^{2+}]_i$ reached > 950 nM, which appeared to result in an apparent desensitization or loss of responsiveness of the K_{Ca} current. Later in the same trace, $[Ca^{2+}]_i$ was estimated to reach 400 nM, which failed to evoke a robust K_{Ca} current. These concentrations are well above the reported threshold for activation of SK3 channels ($EC_{50} \sim 600$ nM) (Barfod et al. 2001; Xia et al. 1998). In the case of the BK HEK293 cell shown in Fig. 8, CCh-evoked $[Ca^{2+}]_i$ spikes reached values of 400–600 nM, which may well be close to or below the threshold for activation of BK, especially at such negative membrane potentials and in the absence of β subunit coexpression ($EC_{50} > 1$ μM). However, there were examples within the same cell (Fig. 10) where $[Ca^{2+}]_i$ spikes activated robust K_{Ca} current spikes, but later within the same trace, similar-magnitude $[Ca^{2+}]_i$ spikes failed to activate robust K_{Ca} currents (current-independent $[Ca^{2+}]_i$ events) or activated diminished K_{Ca} currents. This suggests that at least some of the current-independent Ca^{2+} events may have been due to a reduced responsiveness of K_{Ca} channels to Ca^{2+}, regardless of the threshold for activation.

In summary, these data suggested that the relationship between agonist-evoked dynamic changes in $[Ca^{2+}]_i$ and membrane current is less synchronized in HEK293 STREX cells than in HEK293 SK3 cells or HEK293 hIK1 cells. Moreover, these data could be explained by a dynamic $[Ca^{2+}]_i$ signal-mediated rundown or inhibition of K_{Ca} that occurred more frequently in BK-expressing HEK293 cells.

Discussion

The major aim of the present study was to test whether dynamic changes in $[Ca^{2+}]_i$ differentially regulated different K_{Ca} channel subtypes. This is important in cells such as ECs, salivary acinar cells, and T lymphocytes that not only differentially express these K_{Ca} subtypes but also in which the spatiotemporal shape of $[Ca^{2+}]_i$ signaling has been reported to differentially control cellular function (Berridge et al. 2003; Dolmetsch et al. 1998; Frieden et al. 1999; Giovannucci et al. 2002; Marchenko 2002). In order to study such phenomena, it was necessary to establish a

simplified model cell line with a K_{Ca} null background, so that each overexpressed K_{Ca} subtype can be examined in isolation and exhibit predictable temporally distinct $[Ca^{2+}]_i$ signals that can be experimentally manipulated. We therefore used established HEK293 cell lines that stably expressed SK3, hIK1, or BK (STREX splice variant) channels that responded to agonists (e.g., carbachol) to evoke robust and reproducible temporally distinct $[Ca^{2+}]_i$ oscillations.

The electrophysiological properties of the HEK293 SK3, hIK1, and BK cell lines were characterized by the whole-cell patch clamp technique and exhibited typical SK-, IK-, and BK-like channel properties. All currents were activated by Ca^{2+} and had a reversal potential of −60 mV and a peak current above ~+50 mV. SK-like currents in HEK293 SK3 cells were potentiated by riluzole and inhibited by apamin, whereas IK-like currents in HEK293 hIK1 cells were potentiated by EBIO and inhibited by TRAM34, consistent with previous studies (Barfod et al. 2001; Grunnet et al. 2001; Jensen et al. 1998; Wulff et al. 2000). The STREX splice variant of the BK channel contains a 59-amino acid insert rich in cysteine residues and exhibits a higher Ca^{2+} sensitivity at more hyperpolarizing potentials than other splice variants (Chen et al. 2005). This was therefore chosen for the current study because it was the most likely splice variant of BK to be regulated by dynamic changes in $[Ca^{2+}]_i$ over the physiological range (i.e., submicromolar to several micromolars). K_{Ca} currents in HEK293 BK cells were both Ca^{2+} and voltage dependent and could be activated without added Ca^{2+} in the intracellular solution. BK currents were inhibited by iberiotoxin and enhanced by NS1619, consistent with previous studies (Gribkoff et al. 1996; Jiang et al. 2004a). These data therefore confirm and validate that each K_{Ca}-expressing HEK293 cell line provides a suitable model system to study the effects of dynamic changes in $[Ca^{2+}]_i$ on each K_{Ca} subtype in isolation.

The relationship between $[Ca^{2+}]_i$ and K_{Ca} channels has been extensively studied. However, previous work in the field has focused on investigating the Ca^{2+} sensitivity and Ca^{2+} activation of K_{Ca} channels by monitoring the effects of steady-state $[Ca^{2+}]_i$. This strategy has been implemented to monitor the Ca^{2+} sensitivity of SK1 (Kohler et al. 1996; Xia et al. 1998), SK2 (Hirschberg et al. 1998; Kohler et al. 1996; Xia et al. 1998), SK3 (Barfod et al. 2001; Xia et al. 1998), IK (Ishii et al. 1997; Joiner et al. 1997; Logsdon et al. 1997), and BK channel activity (Ahring et al. 1997; Erxleben et al. 2002). However, physiologically $[Ca^{2+}]_i$ levels within a cell are rarely at a steady state but rather change dynamically, such as during a $[Ca^{2+}]_i$ oscillation. To date, very little information is available about the effects of dynamic changes in $[Ca^{2+}]_i$ on K_{Ca} channel activity yet could provide a greater understanding of how K_{Ca}-dependent processes, such as stimulus-evoked hyperpolarization of ECs, occurs.

Spatiotemporally distinct patterns of $[Ca^{2+}]_i$ signals are important for encoding the specificity of stimulus–response coupling and for ensuring that only certain Ca^{2+}-dependent effectors are activated within a cell. For example, different spatiotemporal $[Ca^{2+}]_i$ signals are important in controlling smooth muscle contraction and relaxation (Nelson et al. 1995), cell cycle progression (Lipskaia and Lompre 2004), and expression of specific sets of genes that control cell differentiation or proliferation (Dolmetsch et al. 1998). Specifically, the frequency of $[Ca^{2+}]_i$ oscillations has been reported to differentially regulate the Ca^{2+}-sensitive transcription factors NFAT, Oct/OAP, and NF-κB (Dolmetsch et al. 1998). Similar mechanisms may exist in ECs, giving rise to differential regulation of K_{Ca} channels and thus hyperpolarization and vasodilation. Different Ca^{2+}-mobilizing agonists can differentially regulate K_{Ca}-dependent EC hyperpolarization, suggesting that different temporal patterns of $[Ca^{2+}]_i$ signal may be responsible. Experiments on rat thoracic aorta demonstrated that acetylcholine-induced and ATP-induced hyperpolarization of the endothelium occurred via selective activation of IK and SK channels, respectively (Marchenko 2002). Additionally, in cultured porcine coronary artery ECs, substance P and bradykinin selectively activated SK and BK channels, respectively, to induce hyperpolarization (Frieden et al. 1999). It has also been shown that acetylcholine-induced hyperpolarization in uncontracted rat mesenteric artery occurred solely via the activation of SK channels, whereas in contracted arteries, both SK and IK channels contributed (Crane et al. 2003). The mechanism underlying the selective activation of IK and SK channels was unknown in all these cases. However, the $[Ca^{2+}]_i$ responses produced by substance P and bradykinin in the experiments performed by Frieden et al. (1999) differed in their amplitude and temporal properties, which could underlie the differential activation of IK and SK channels.

In the current study, all patterns of $[Ca^{2+}]_i$ signal evoked by Ca^{2+}-mobilizing agonists were able to activate each K_{Ca} channel subtype. We had hypothesized that because of their differing Ca^{2+} sensitivities and mechanisms of Ca^{2+} activation, different K_{Ca} channel subtypes would respond differently to temporally distinct patterns of dynamic $[Ca^{2+}]_i$ signals, especially because BK channels bind directly to Ca^{2+} and SK/IK channels bind indirectly to Ca^{2+} via calmodulin. For any given K_{Ca} subtype, there was no clear-cut selective activation of K_{Ca} current by any specific pattern of $[Ca^{2+}]_i$ signal, nor did there appear to be any summation of channel activity during fast $[Ca^{2+}]_i$ oscillations, as one would expect for different on and off Ca^{2+} binding rates. In fact, during fast frequency oscillations or when $[Ca^{2+}]_i$ oscillations started to fuse into a peak and

plateau response, there appeared in some cells to be an apparent inactivation of K_{Ca} channel activity rather than a summation of the current. However, the number of cells that exhibited high-frequency oscillations or peak and plateau responses was low, which therefore made quantification of the data difficult.

However, there were differences observed in the relationship between agonist-evoked dynamic changes in $[Ca^{2+}]_i$ and K_{Ca} current between subtypes. In less than half of the cells tested (regardless of K_{Ca} channel expression), there was a general trend for the membrane current to follow the pattern of the $[Ca^{2+}]_i$ signal. However, there was also evidence in some cells of Ca^{2+}-independent current events and/or current-independent $[Ca^{2+}]_i$ events.

A substantial number of Ca^{2+}-independent current events occurred in all three HEK293 K_{Ca}-expressing cell lines. These were particularly high in HEK293 hIK1 cells and HEK293 BK cells in which almost half of all current events occurred in the absence of a change in $[Ca^{2+}]_i$. This observation may be due to a limitation in the experimental equipment. Technical constraints made it impossible to simultaneously measure K_{Ca} currents and the spatial properties of agonist-evoked $[Ca^{2+}]_i$ signals, for example by imaging indo-1 or fura-2 fluorescence. Instead, indo-1 fluorescence was recorded using a photomultiplier-based detection system with an aperture that enclosed the bulk of a single cell that was simultaneously patch clamped using the whole-cell perforated patch technique. Therefore, only changes in average $[Ca^{2+}]_i$ across the entire cell were monitored. This means that only global changes in $[Ca^{2+}]_i$ were likely large enough to register as a $[Ca^{2+}]_i$ peak. Any local increases in $[Ca^{2+}]_i$ occurring within microdomains sufficient to activate nearby K_{Ca} channels and thus register as a change in current may be effectively masked or diminished when averaged across the entire cell. This was particularly the case for HEK293 BK cells, where changes in current occasionally corresponded to very small blips in $[Ca^{2+}]_i$ that could represent local changes in $[Ca^{2+}]_i$ evoking spontaneous transient outward currents. BK channels in particular are well known for being activated by local increases in $[Ca^{2+}]_i$ within microdomains to produce spontaneous transient outward currents (Nelson et al. 1995; Zhuge et al. 2002). Therefore, it is possible that not all Ca^{2+}-independent current events were truly Ca^{2+} independent.

However, when fura-2-loaded intact (nonpatched) cells were imaged with a CCD camera, none of the K_{Ca}-expressing HEK293 cell lines exhibited bona fide localized agonist-evoked $[Ca^{2+}]_i$ signals that alone could explain all of the Ca^{2+}-independent current events observed. In fact, most cells (all of IK- and SK-expressing cells) exhibited rapid global $[Ca^{2+}]_i$ waves that initiated at one end of the cell and rapidly propagated to the opposite end of the cell within a few seconds. In some cells (e.g., HEK293 BK cells) that were likely tightly coupled and exhibited a more projection-like morphology, CCh evoked slower global $[Ca^{2+}]_i$ waves. These $[Ca^{2+}]_i$ signals initiated within projection-like regions of the cell and propagated more slowly to the opposite end of the cell body over several seconds (Fig. 9). Such spatiotemporal $[Ca^{2+}]_i$ waves could give rise to apparent desynchronized $[Ca^{2+}]_i$ -signal dependent K_{Ca} currents. Therefore, depending on the spatial distribution of K_{Ca} channels, a $[Ca^{2+}]_i$ signal in a projection may be sensed by K_{Ca} channels in that region and thus activate a robust whole-cell K_{Ca} current, which may occur several seconds before the $[Ca^{2+}]_i$ wave propagating to the bulk of the soma. This would lead to K_{Ca} currents that were several seconds out of phase of the bulk global $[Ca^{2+}]_i$. Although such phenomena could explain some of the Ca^{2+}-independent current events, they are unlikely to explain all Ca^{2+}-independent current events, especially those that occurred several tens of seconds out of phase of any $[Ca^{2+}]_i$ signal in some cells. Moreover, only uncoupled single cells that were free of extensive projections were selected for patch clamp experiments, and these types of cells never exhibited such complex spatiotemporal $[Ca^{2+}]_i$ waves.

One explanation for the differences in the number of Ca^{2+}-independent current events between HEK293 hIK1, HEK293 SK3, and HEK293 BK cells could be due to the differing Ca^{2+} sensitivities of the channels. IK channels are more sensitive to Ca^{2+} than SK3 channels (Barfod et al. 2001; Ishii et al. 1997; Joiner et al. 1997; Logsdon et al. 1997; Xia et al. 1998) and may therefore be activated more frequently by local changes in $[Ca^{2+}]_i$. However, BK is reported to have a much lower sensitivity to Ca^{2+} in the micromolar range (Petrik and Brenner 2007) and yet exhibit a similar number of Ca^{2+}-independent current events. Alternatively, the difference could be due to spatial localization of the different K_{Ca} subtypes to different sources of the $[Ca^{2+}]_i$ signal, which is not unprecedented in other cell types. Recent studies suggest that IK1 may functionally couple to acetylcholine-induced Ca^{2+} release from IP_3R, whereas SK3 couples to shear stress-induced Ca^{2+} entry through TRPV4 channels in ECs (Brahler et al. 2009; Sankaranarayanan et al. 2009). This may provide alternative routes of hyperpolarization, and thus vasodilation, induced by different physiological stimuli via the selective activation of specific K_{Ca} subtypes within the same cell. In rat mesenteric artery, IK1 was found localized to endothelial projections that couple with smooth muscle cells via myoendothelial gap junctions, whereas SK3 was found at the borders between adjacent ECs (Sandow et al. 2006). Furthermore, there is evidence that SK3, but not IK channels, reside within endothelial caveolae and differentially regulate vascular tone in rat mesenteric and porcine

coronary artery (Absi et al. 2007). Furthermore, BK channels have also been shown to reside within caveolae in human myometrial smooth muscle cells (Brainard et al. 2005), bovine aortic ECs (Wang et al. 2005) and glioma cells, where they functionally couple to IP_3Rs and thus Ca^{2+} release (Weaver et al. 2007). However, the current study provides no direct evidence for such differential spatial regulation of K_{Ca} channels and because these channels have been recombinantly overexpressed it is more likely that the K_{Ca} channels are abundant in all regions of the plasma membrane.

Although some Ca^{2+}-independent current events could be explained by localized $[Ca^{2+}]_i$ signals or slowly propagating spatiotemporal $[Ca^{2+}]_i$ waves, current-independent $[Ca^{2+}]_i$ events, on the other hand, can be explained more reliably by a true uncoupling of K_{Ca} current from $[Ca^{2+}]_i$ signal. The relationship between dynamic changes in $[Ca^{2+}]_i$ and K_{Ca} channel activity appeared to be most synchronized in HEK293 SK3 and HEK293 hIK1 cells and least synchronized in HEK293 BK cells. In HEK293 SK3 cells and HEK293 hIK1 cells, almost all $[Ca^{2+}]_i$ peaks elicited a change in current; however, just over a third of all $[Ca^{2+}]_i$ events failed to elicit a change in current in HEK293 BK cells. This could simply reflect the differences in Ca^{2+} sensitivity of the channels. BK channels are activated by micromolar $[Ca^{2+}]$ (Petrik and Brenner 2007), while SK and IK channels are activated by nanomolar $[Ca^{2+}]$ (Ishii et al. 1997; Joiner et al. 1997; Xia et al. 1998). IK channels are the most Ca^{2+} sensitive of the K_{Ca} channels (K_d = 100–300 nm) (Ishii et al. 1997; Joiner et al. 1997; Logsdon et al. 1997), whereas the K_d for SK3 channels is approximately 600–700 nm (Barfod et al. 2001; Xia et al. 1998). However, an important observation from the current study is that repetitive $[Ca^{2+}]_i$ spikes of similar magnitude were often observed to activate robust K_{Ca} currents at the beginning of the trace and then completely failed to activate any current later on in the experiment even in the same cell. This suggests that at least some of the current-independent $[Ca^{2+}]_i$ events may be due to either a Ca^{2+}-dependent inactivation or the current losing responsiveness, perhaps the result of a dynamic $[Ca^{2+}]_i$ signal-dependent inhibition or desensitization of the K_{Ca} channel. The lack of $[Ca^{2+}]_i$-current synchronization and the greater occurrence of current-independent $[Ca^{2+}]_i$ events in HEK293 BK cells suggests that the BK_{STREX} channel variant may be more prone to such Ca^{2+}-dependent inactivation or $[Ca^{2+}]_i$ signal-dependent inhibition. Such intrinsic inactivation of the K_{Ca} channel, Ca^{2+} dependent or otherwise, is difficult to reconcile with the whole cell patch clamp experiments in Figs. 2 and 4, which show no inactivation at least over the short time course (100 ms) of current measurements. However, we cannot rule out the possibility of longer-term inactivation, which may occur over several seconds to several minutes for all three KCa channels. Interestingly, however, there is evidence that BK channels, but not SK3 or IK channels, may undergo a Ca^{2+}-dependent inactivation that may explain some of the current-independent Ca^{2+} events. Specifically, studies that used single-channel recordings from inside-out patches of rat hippocampal neurons showed that BK channels undergo Ca^{2+}-dependent inactivation in the presence of as low as 1 μM Ca^{2+} (Hicks and Marrion 1998). This was suggested to be due to the physical occlusion of the channel pore by an associated particle, acting from the cytosolic side of the channel. Later studies have suggested that this may involve a β subunit (Wallner et al. 1999), although this could not account for the regulation of BK channels in HEK293 BK cells in the current study because β subunit were not coexpressed. Moreover, such a phenomenon is also more difficult to explain for SK3 channels for which such intrinsic Ca^{2+}-dependent inactivation has never been reported.

Another explanation for the observed loss of responsiveness of K_{Ca} currents (as for SK3 in Fig. 7), despite $[Ca^{2+}]_i$ reaching suprathreshold concentrations, could be attributed to the dynamic $[Ca^{2+}]_i$ signal regulation of a downstream signaling pathway that inhibits or desensitizes the K_{Ca} channel. Such signaling pathways could include a Ca^{2+}-dependent kinase, such as protein kinase C (PKC) and/or Ca^{2+}/Calmodulin-dependent kinases (CaMK), or a Ca^{2+}-dependent phosphatase, such as calcineurin. Evidence for the regulation of K_{Ca} channels by PKC has been somewhat contradictory and likely depends on the cellular context. BK channel activity has been shown to be both inhibited (Schubert et al. 1999) and activated (Kim and Park 2008) by PKC. Likewise, PKC has also been reported to inhibit IK in human erythrocytes (Del Carlo et al. 2003) and activate IK in arterial smooth muscle cells (Hayabuchi et al. 2006). SK channels in HTC hepatoma cells have been shown to be activated, rather than inhibited by PKC (Wang et al. 1996). It is of particular interest that CaMKII, which is differentially regulated by the frequency of $[Ca^{2+}]_i$ oscillations (De Koninck and Schulman 1998), has been reported to be responsible for the Ca^{2+}-dependent inhibition of endogenous apical K_{Ca} conductance in rat cortical collecting duct cells (Kubokawa et al. 1995). Moreover, the Ca^{2+}-dependent phosphatase calcineurin has been shown to inhibit BK channels by the direct association with the channel (Loane et al. 2006). It is therefore possible that during high-frequency $[Ca^{2+}]_i$ oscillations or when oscillations fuse into a sustained increase in $[Ca^{2+}]_i$ (e.g., Fig. 7), CaMK or calcineurin may contribute to the desensitization of K_{Ca} channels (as observed for SK3 HEK293 cells in Fig. 7), or even contribute to the current-independent Ca^{2+} events (as observed for SK3 and BK HEK293 cells, Figs. 7, 10). Furthermore, activation of

hIK1 expressed in HEK293 cells was unaffected by protein PKC or CaMKII inhibitors (Gerlach et al. 2000). This is broadly in line with our own current data whereby hIK1-expressing HEK293 cells exhibited negligible current-independent Ca^{2+} events and K_{Ca} currents were the most synchronized with dynamic $[Ca^{2+}]_i$ signals. However, the current study provides no direct molecular evidence for the regulation, or dysregulation, of K_{Ca} channels by dynamic $[Ca^{2+}]_i$ signaling, which is beyond the scope of the current study but clearly warrants further investigation.

It is also important to note that endogenous BK channels are likely to be coexpressed with β subunits in native cells. Unlike SK and IK channels, BK channels are modulated allosterically by Ca^{2+}, voltage, and β subunits that have been reported to affect both the voltage and Ca^{2+} dependency of the channel (Cox and Aldrich 2000; Latorre and Brauchi 2006; Perez et al. 1993; Petrik and Brenner 2007; Wallner et al. 1995). In fact, in β1-knockout mice, arterial smooth muscle BK channels become unresponsive to localized Ca^{2+} sparks (Brenner et al. 2000b). The pore-forming α subunit, when expressed alone, exhibits very little activity at negative potentials (cells clamped at 60 mV; Fig. 4d). Therefore, it is possible that the K_{Ca} currents observed under perforated patch clamp conditions in the present study arise from the BK channels experiencing very high $[Ca^{2+}]$ very close to Ca^{2+} release sites, and so by definition may be uncoupled from global $[Ca^{2+}]_i$ signals. This may help to explain the large degree of desynchronicity between K_{Ca} currents and $[Ca^{2+}]_i$ signaling in BK HEK293 cells. Different results might be obtained under conditions where the channels would be allosterically sensitized to Ca^{2+}, i.e., at more positive membrane potentials or if the β subunit is coexpressed. Therefore, care must be taken when extrapolating the effects of dynamic $[Ca^{2+}]_i$ signal-mediated regulation of recombinantly expressed BK from the current study, where β subunits were not coexpressed, to the regulation of endogenous BK in native cells.

In summary, we provide the first comprehensive study that examines the effects of dynamic changes in $[Ca^{2+}]_i$ on three mechanistically distinct K_{Ca} channel subtypes, SK3, hIK1, and the BK_{STREX} splice variant of the BK channel. Although in a large proportion of cells K_{Ca} currents faithfully followed $[Ca^{2+}]_i$, there was also a large degree of desynchronization between $[Ca^{2+}]_i$ and K_{Ca} current that varied between K_{Ca} subtypes. This desynchronization was most evident in HEK293 BK cells and was most likely due to a dynamic $[Ca^{2+}]_i$ signal-dependent inhibition or desensitization of the K_{Ca} channel. This observation would not be revealed using conventional methods of measuring whole-cell K_{Ca} currents, whereby $[Ca^{2+}]$ is buffered to a steady-state concentration within a patch pipette. These phenomena are likely important for encoding stimulus–response coupling in cells such as ECs, T lymphocytes, and epithelial cells that differentially express these K_{Ca} subtypes. The molecular mechanisms that control these phenomena clearly warrant further investigation.

Acknowledgments This work was supported by a BBSRC grant awarded to J. I. E. Bruce and a BHF grant awarded to I. M. Fearon. The authors thank Dr. Frank Graham (McMaster University) for HEK293 cells, Dr. Gary Willars (University of Leicester) for HEK293 M3 cells, Dr. Dan Devor (University of Pittsburgh) for HEK293 hIK1 cells, Dr. Steve Lidofsky (University of Vermont) for HEK293 SK3, and Prof. Mike Shipston (University of Edinburgh) for the STREX DNA.

References

Absi M, Burnham MP, Weston AH, Harno E, Rogers M, Edwards G (2007) Effects of methyl beta-cyclodextrin on EDHF responses in pig and rat arteries; association between SK_{Ca} channels and caveolin-rich domains. Br J Pharmacol 151:332–340

Ahring PK, Strobaek D, Christophersen P, Olesen SP, Johansen TE (1997) Stable expression of the human large-conductance Ca^{2+}-activated K^+ channel alpha- and beta-subunits in HEK293 cells. FEBS Lett 415:67–70

Barfod ET, Moore AL, Lidofsky SD (2001) Cloning and functional expression of a liver isoform of the small conductance Ca^{2+}-activated K^+ channel SK3. Am J Physiol Cell Physiol 280:C836–C842

Berridge MJ, Bootman MD, Roderick HL (2003) Calcium signalling: dynamics, homeostasis and remodelling. Nat Rev Mol Cell Biol 4:517–529

Brahler S, Kaistha A, Schmidt VJ, Wolfle SE, Busch C, Kaistha BP, Kacik M, Hasenau AL, Grgic I, Si H, Bond CT, Adelman JP, Wulff H, de Wit C, Hoyer J, Kohler R (2009) Genetic deficit of SK3 and IK1 channels disrupts the endothelium-derived hyperpolarizing factor vasodilator pathway and causes hypertension. Circulation 119:2323–2332

Brainard AM, Miller AJ, Martens JR, England SK (2005) Maxi-K channels localize to caveolae in human myometrium: a role for an actin–channel–caveolin complex in the regulation of myometrial smooth muscle K^+ current. Am J Physiol Cell Physiol 289:C49–C57

Brenner R, Jegla TJ, Wickenden A, Liu Y, Aldrich RW (2000a) Cloning and functional characterization of novel large conductance calcium-activated potassium channel beta subunits, hKCNMB3 and hKCNMB4. J Biol Chem 275:6453–6461

Brenner R, Perez GJ, Bonev AD, Eckman DM, Kosek JC, Wiler SW, Patterson AJ, Nelson MT, Aldrich RW (2000b) Vasoregulation by the beta1 subunit of the calcium-activated potassium channel. Nature 407:870–876

Chen L, Tian L, MacDonald SH, McClafferty H, Hammond MS, Huibant JM, Ruth P, Knaus HG, Shipston MJ (2005) Functionally diverse complement of large conductance calcium- and voltage-activated potassium channel (BK) alpha-subunits generated from a single site of splicing. J Biol Chem 280:33599–33609

Cox DH, Aldrich RW (2000) Role of the beta1 subunit in large-conductance Ca^{2+}-activated K^+ channel gating energetics. Mechanisms of enhanced Ca^{2+} sensitivity. J Gen Physiol 116:411–432

Crane GJ, Gallagher N, Dora KA, Garland CJ (2003) Small- and intermediate-conductance calcium-activated K^+ channels provide different facets of endothelium-dependent hyperpolarization in rat mesenteric artery. J Physiol 553:183–189

De Koninck P, Schulman H (1998) Sensitivity of CaM kinase II to the frequency of Ca^{2+} oscillations. Science 279:227–230

Del Carlo B, Pellegrini M, Pellegrino M (2003) Modulation of Ca^{2+}-activated K^+ channels of human erythrocytes by endogenous protein kinase C. Biochim Biophys Acta 1612:107–116

Dolmetsch RE, Xu K, Lewis RS (1998) Calcium oscillations increase the efficiency and specificity of gene expression. Nature 392: 933–936

Erxleben C, Everhart AL, Romeo C, Florance H, Bauer MB, Alcorta DA, Rossie S, Shipston MJ, Armstrong DL (2002) Interacting effects of N-terminal variation and strex exon splicing on slo potassium channel regulation by calcium, phosphorylation, and oxidation. J Biol Chem 277:27045–27052

Faber ES, Sah P (2003) Calcium-activated potassium channels: multiple contributions to neuronal function. Neuroscientist 9: 181–194

Frieden M, Sollini M, Beny J (1999) Substance P and bradykinin activate different types of K_{Ca} currents to hyperpolarize cultured porcine coronary artery endothelial cells. J Physiol 519(pt 2): 361–371

Frieden M, Malli R, Samardzija M, Demaurex N, Graier WF (2002) Subplasmalemmal endoplasmic reticulum controls K(Ca) channel activity upon stimulation with a moderate histamine concentration in a human umbilical vein endothelial cell line. J Physiol 540:73–84

Gerlach AC, Gangopadhyay NN, Devor DC (2000) Kinase-dependent regulation of the intermediate conductance, calcium-dependent potassium channel, hIK1. J Biol Chem 275:585–598

Giovannucci DR, Bruce JI, Straub SV, Arreola J, Sneyd J, Shuttleworth TJ, Yule DI (2002) Cytosolic Ca(2+) and Ca(2+)-activated Cl(−) current dynamics: insights from two functionally distinct mouse exocrine cells. J Physiol 540:469–484

Gribkoff VK, Lum-Ragan JT, Boissard CG, Post-Munson DJ, Meanwell NA, Starrett JE Jr, Kozlowski ES, Romine JL, Trojnacki JT, McKay MC, Zhong J, Dworetzky SI (1996) Effects of channel modulators on cloned large-conductance calcium-activated potassium channels. Mol Pharmacol 50:206–217

Gribkoff VK, Starrett JE Jr, Dworetzky SI (2001) Maxi-K potassium channels: form, function, and modulation of a class of endogenous regulators of intracellular calcium. Neuroscientist 7: 166–177

Grunnet M, Jespersen T, Angelo K, Frokjaer-Jensen C, Klaerke DA, Olesen SP, Jensen BS (2001) Pharmacological modulation of SK3 channels. Neuropharmacology 40:879–887

Grynkiewicz G, Poenie M, Tsien RY (1985) A new generation of Ca^{2+} indicators with greatly improved fluorescence properties. J Biol Chem 260:3440–3450

Gutman GA, Chandy KG, Adelman JP, Aiyar J, Bayliss DA, Clapham DE, Covarriubias M, Desir GV, Furuichi K, Ganetzky B, Garcia ML, Grissmer S, Jan LY, Karschin A, Kim D, Kuperschmidt S, Kurachi Y, Lazdunski M, Lesage F, Lester HA, McKinnon D, Nichols CG, O'Kelly I, Robbins J, Robertson GA, Rudy B, Sanguinetti M, Seino S, Stuehmer W, Tamkun MM, Vandenberg CA, Wei A, Wulff H, Wymore RS (2003) International Union of Pharmacology. XLI. Compendium of voltage-gated ion channels: potassium channels. Pharmacol Rev 55:583–586

Hardie RC (2007) TRP channels and lipids: from *Drosophila* to mammalian physiology. J Physiol 578:9–24

Hayabuchi Y, Nakaya Y, Yasui S, Mawatari K, Mori K, Suzuki M, Kagami S (2006) Angiotensin II activates intermediate-conductance Ca^{2+}-activated K^+ channels in arterial smooth muscle cells. J Mol Cell Cardiol 41:972–979

Hicks GA, Marrion NV (1998) Ca^{2+}-dependent inactivation of large conductance Ca^{2+}-activated K^+ (BK) channels in rat hippocampal neurones produced by pore block from an associated particle. J Physiol 508(pt 3):721–734

Hirschberg B, Maylie J, Adelman JP, Marrion NV (1998) Gating of recombinant small-conductance Ca^{2+}-activated K^+ channels by calcium. J Gen Physiol 111:565–581

Horn R, Marty A (1988) Muscarinic activation of ionic currents measured by a new whole-cell recording method. J Gen Physiol 92:145–159

Ishii TM, Silvia C, Hirschberg B, Bond CT, Adelman JP, Maylie J (1997) A human intermediate conductance calcium-activated potassium channel. Proc Natl Acad Sci USA 94:11651–11656

Jensen BS, Strobaek D, Christophersen P, Jorgensen TD, Hansen C, Silahtaroglu A, Olesen SP, Ahring PK (1998) Characterization of the cloned human intermediate-conductance Ca^{2+}-activated K^+ channel. Am J Physiol 275:C848–C856

Jiang B, Cao K, Wang R (2004a) Inhibitory effect of protopine on K_{ATP} channel subunits expressed in HEK293 cells. Eur J Pharmacol 506:93–100

Jiang B, Hattori N, Liu B, Nakayama Y, Kitagawa K, Inagaki C (2004b) Suppression of cell proliferation with induction of p21 by Cl^- channel blockers in human leukemic cells. Eur J Pharmacol 488:27–34

Joiner WJ, Wang LY, Tang MD, Kaczmarek LK (1997) hSK4, a member of a novel subfamily of calcium-activated potassium channels. Proc Natl Acad Sci USA 94:11013–11018

Jones HM, Hamilton KL, Devor DC (2005) Role of an S4–S5 linker lysine in the trafficking of the Ca(2+)-activated K(+) channels IK1 and SK3. J Biol Chem 280:37257–37265

Kim JY, Park CS (2008) Potentiation of large-conductance calcium-activated potassium (BK_{Ca}) channels by a specific isoform of protein kinase C. Biochem Biophys Res Commun 365:459–465

Kohler M, Hirschberg B, Bond CT, Kinzie JM, Marrion NV, Maylie J, Adelman JP (1996) Small-conductance, calcium-activated potassium channels from mammalian brain. Science 273: 1709–1714

Kubokawa M, Wang W, McNicholas CM, Giebisch G (1995) Role of Ca^{2+}/CaMK II in $Ca^{(2+)}$-induced K^+ channel inhibition in rat CCD principal cell. Am J Physiol 268:F211–F219

Latorre R, Brauchi S (2006) Large conductance Ca^{2+}-activated K^+ (BK) channel: activation by Ca^{2+} and voltage. Biol Res 39: 385–401

Ledoux J, Werner ME, Brayden JE, Nelson MT (2006) Calcium-activated potassium channels and the regulation of vascular tone. Physiology (Bethesda) 21:69–78

Lippiat JD, Standen NB, Harrow ID, Phillips SC, Davies NW (2003) Properties of BK(Ca) channels formed by bicistronic expression of hSloalpha and beta1–4 subunits in HEK293 cells. J Membr Biol 192:141–148

Lipskaia L, Lompre AM (2004) Alteration in temporal kinetics of Ca^{2+} signalling and control of growth and proliferation. Biol Cell 96:55–68

Loane DJ, Hicks GA, Perrino BA, Marrion NV (2006) Inhibition of BK channel activity by association with calcineurin in rat brain. Eur J Neurosci 24:433–441

Logsdon NJ, Kang J, Togo JA, Christian EP, Aiyar J (1997) A novel gene, $hK_{Ca}4$, encodes the calcium-activated potassium channel in human T lymphocytes. J Biol Chem 272:32723–32726

Marchenko SM (2002) Acetylcholine and ATP hyperpolarize endothelium via activation of different types of Ca^{2+}-activated K^+ channels. Bull Exp Biol Med 134:422–424

McCartney CE, McClafferty H, Huibant JM, Rowan EG, Shipston MJ, Rowe IC (2005) A cysteine-rich motif confers hypoxia sensitivity to mammalian large conductance voltage- and Ca^{2+}-activated K^+ (BK) channel alpha-subunits. Proc Natl Acad Sci USA 102:17870–17876

Melvin JE, Yule D, Shuttleworth T, Begenisich T (2005) Regulation of fluid and electrolyte secretion in salivary gland acinar cells. Annu Rev Physiol 67:445–469

Nelson MT, Cheng H, Rubart M, Santana LF, Bonev AD, Knot HJ, Lederer WJ (1995) Relaxation of arterial smooth muscle by calcium sparks. Science 270:633–637

Perez GJ, Toro L, Erulkar SD, Stefani E (1993) Characterization of large-conductance, calcium-activated potassium channels from human myometrium. Am J Obstet Gynecol 168:652–660

Petrik D, Brenner R (2007) Regulation of STREX exon large conductance, calcium-activated potassium channels by the beta-4 accessory subunit. Neuroscience 149:789–803

Saito M, Nelson C, Salkoff L, Lingle CJ (1997) A cysteine-rich domain defined by a novel exon in a slo variant in rat adrenal chromaffin cells and PC12 cells. J Biol Chem 272:11710–11717

Saleem F, Rowe IC, Shipston MJ (2009) Characterization of BK channel splice variants using membrane potential dyes. Br J Pharmacol 156:143–152

Sandow SL, Neylon CB, Chen MX, Garland CJ (2006) Spatial separation of endothelial small- and intermediate-conductance calcium-activated potassium channels (K_{Ca}) and connexins: possible relationship to vasodilator function? J Anat 209: 689–698

Sankaranarayanan A, Raman G, Busch C, Schultz T, Zimin PI, Hoyer J, Kohler R, Wulff H (2009) Naphtho[1, 2-d]thiazol-2-ylamine (SKA-31), a new activator of KCa2 and KCa3.1 potassium channels, potentiates the endothelium-derived hyperpolarizing factor response and lowers blood pressure. Mol Pharmacol 75:281–295

Schubert R, Noack T, Serebryakov VN (1999) Protein kinase C reduces the K_{Ca} current of rat tail artery smooth muscle cells. Am J Physiol 276:C648–C658

Shipston MJ, Duncan RR, Clark AG, Antoni FA, Tian L (1999) Molecular components of large conductance calcium-activated potassium (BK) channels in mouse pituitary corticotropes. Mol Endocrinol 13:1728–1737

Soboloff J, Spassova M, Hewavitharana T, He LP, Luncsford P, Xu W, Venkatachalam K, van Rossum D, Patterson RL, Gill DL (2007) TRPC channels: integrators of multiple cellular signals. Handb Exp Pharmacol 179:575–591

Stocker M (2004) Ca^{2+}-activated K^+ channels: molecular determinants and function of the SK family. Nat Rev Neurosci 5: 758–770

Wallner M, Meera P, Ottolia M, Kaczorowski GJ, Latorre R, Garcia ML, Stefani E, Toro L (1995) Characterization of and modulation by a beta-subunit of a human maxi KCa channel cloned from myometrium. Receptors Channels 3:185–199

Wallner M, Meera P, Toro L (1999) Molecular basis of fast inactivation in voltage and Ca^{2+}-activated K^+ channels: a transmembrane beta-subunit homolog. Proc Natl Acad Sci USA 96:4137–4142

Wang Y, Sostman A, Roman R, Stribling S, Vigna S, Hannun Y, Raymond J, Fitz JG (1996) Metabolic stress opens K^+ channels in hepatoma cells through a Ca^{2+}- and protein kinase C alpha–dependent mechanism. J Biol Chem 271:18107–18113

Wang XL, Ye D, Peterson TE, Cao S, Shah VH, Katusic ZS, Sieck GC, Lee HC (2005) Caveolae targeting and regulation of large conductance Ca^{2+}-activated K^+ channels in vascular endothelial cells. J Biol Chem 280:11656–11664

Weaver AK, Olsen ML, McFerrin MB, Sontheimer H (2007) BK channels are linked to inositol 1, 4, 5-triphosphate receptors via lipid rafts: a novel mechanism for coupling [Ca2+]i to ion channel activation. J Biol Chem 282:31558–31568

Wiecha J, Munz B, Wu Y, Noll T, Tillmanns H, Waldecker B (1998) Blockade of Ca^{2+}-activated K^+ channels inhibits proliferation of human endothelial cells induced by basic fibroblast growth factor. J Vasc Res 35:363–371

Wulff H, Miller MJ, Hansel W, Grissmer S, Cahalan MD, Chandy KG (2000) Design of a potent and selective inhibitor of the intermediate-conductance Ca^{2+}-activated K^+ channel, $IK_{Ca}1$: a potential immunosuppressant. Proc Natl Acad Sci USA 97:8151–8156

Xia XM, Fakler B, Rivard A, Wayman G, Johnson-Pais T, Keen JE, Ishii T, Hirschberg B, Bond CT, Lutsenko S, Maylie J, Adelman JP (1998) Mechanism of calcium gating in small-conductance calcium-activated potassium channels. Nature 395:503–507

Yang J, Williams JA, Yule DI, Logsdon CD (1995) Mutation of carboxyl-terminal threonine residues in human M3 muscarinic acetylcholine receptor modulates the extent of sequestration and desensitization. Mol Pharmacol 48:477–485

Zhuge R, Fogarty KE, Tuft RA, Walsh JV Jr (2002) Spontaneous transient outward currents arise from microdomains where BK channels are exposed to a mean Ca^{2+} concentration on the order of 10 microM during a Ca^{2+} spark. J Gen Physiol 120:15–27